Tectonophysics 871 (2024) 230170

Contents lists available at ScienceDirect

Tectonophysics

journal homepage: www.elsevier.com/locate/tecto

High-resolution geophysical investigations in the central Apennines seismic belt (Italy): Results from the Campo Felice tectonic basin

F. Villani [a,*], S. Maraio [a], L. Improta [a], V. Sapia [a], G. Di Giulio [a], P. Baccheschi [a], M. Pischiutta [a], M. Vassallo [a], V. Materni [a], P.P. Bruno [b], C.A. Brunori [a], R. Civico [a], A. D'Alessandro [a], C. Felicetta [a], S. Lovati [a], T. Ricci [a], S. Scudero [a], P.M. De Martini [a]

[a] Istituto Nazionale di Geofisica e Vulcanologia, Italy
[b] University of Naples Federico II, Italy

ARTICLE INFO

Keywords:
Central Apennines
Extensional basin
Normal fault
Active-source seismic profiling
Electrical resistivity tomography
Ambient noise

ABSTRACT

The Campo Felice basin, in the central Apennines seismic belt (Italy), developed in the hangingwall of a 30 km-long system of NW-trending normal faults with Holocene paleoseismic activity and potential sources of M 6–7 earthquakes. We provide the first subsurface images of a key portion of the basin bounded by the Mt. Cefalone fault along two intersecting profiles trending NNE-SSW (CF-Dip, 1195 m-long) and WNW-ESE (CF-Strike, 1315-m long). We combined high-resolution depth-migrated reflection sections with P-wave velocity and electrical resistivity tomography models. CF-Dip profile displays a wedge-like syn-tectonic sedimentary sequence of alluvial and glacial deposits with Vp ~ 2500–3000 m/s and resistivity > 500 Ωm in the hangingwall of Mt. Cefalone fault, overlying a high-Vp (>4000 m/s) limestone bedrock ~ 300 m deep. The whole sequence displays reflectors truncated by the Mt. Cefalone fault zone and subsidiary antithetic faults. CF-Strike profile, tied to three 80–110 m-deep boreholes, shows a thick fluvio-lacustrine sequence with low-Vp (<2000 m/s) and low resistivity (<100 Ωm), and a bedrock that deepens to the southeast (>450 m). Single-station ambient noise measurements display Horizontal to Vertical Spectral Ratios with peaks at ~1 Hz, decreasing to ~0.8 Hz to the southeast in agreement with the bedrock deepening indicated by seismic profiling. According to our results, the Campo Felice basin is a deep asymmetric half-graben controlled by faulting whose activity likely started before the Middle Pleistocene. Our minimum displacement estimate accrued in the past 0.5 Ma by the Mt. Cefalone fault is in the range of ~100–250 m.

1. Introduction

In the framework of the tectonically active zones of the circum-Mediterranean orogens, the central Apennines (Italy) represent a well-known example of a Cenozoic fold-and-thrust-belt affected by post-orogenic extensional tectonics (*e.g.*, Ghisetti and Vezzani, 1999). Geological data suggest that extension initiated in the late Pliocene (*e.g.*, Cosentino et al., 2017) and involved a large part of the chain throughout the Quaternary (*e.g.*, Galadini and Galli, 2000). Current NE-directed extension with rates of ~1–2.5 mm/a documented by geodetic data (*e.g.*, D'Agostino et al. 2011; Serpelloni et al., 2022) is partitioned into an array of segmented normal faults, typically NW-SE oriented (Boncio et al., 2004; Cowie and Roberts, 2001; Cowie et al., 2017). Active extension is responsible for strong seismic sequences (magnitude up to M ~ 6.5–7) that repeatedly hit the belt axial zone in the last centuries, with thousands of victims and dramatic socio-economic consequences (Fig. 1; *e.g.*, Chiarabba et al. 2020). As such, active seismogenic normal faults represent a major threat in central Italy.

The long-term activity of the normal faults in the central Apennines promoted the development of intramontane extensional basins mostly expressed as half-grabens (*e.g.*, Schlische, 1991), developed throughout the Plio-Quaternary (D'Agostino et al. 2011; Geurts et al., 2018). As with most fault-controlled depressions, the accommodation space in the hangingwall volume of the Apennines extensional basins stores sediments delivered by rivers, including clastic input from the surrounding uplifted blocks (*e.g.*, Gawthorpe and Leeder, 2000; Gallen and Wegmann, 2017). Additionally, the spatial pattern of displacement of the bounding faults controls the basins' shape and size (Bull, 2009;

* Corresponding author.
E-mail address: fabio.villani@ingv.it (F. Villani).

https://doi.org/10.1016/j.tecto.2023.230170
Received 28 July 2023; Received in revised form 13 November 2023; Accepted 7 December 2023
Available online 13 December 2023

Whittaker et al., 2008; Burbank and Anderson, 2011). Therefore, they embody a geological record of fault growth history, modulated by the interplay of tectonics and erosional/depositional processes (Manighetti et al. 2001; Nicol et al. 2010; Nixon et al. 2014). From these relations, it is clear that a comprehensive understanding of normal fault growth processes, including a correct assessment of their degree of activity and seismogenic potential, requires a detailed knowledge of the subsurface structure and depositional architecture of their hangingwall basins.

In the central Apennines, the study of the deformation history of active normal faults is usually based on surface geological and paleoseismic data that cover different time intervals (Galli et al. 2008; Faure Walker et al., 2021). Unfortunately, a significant portion of the sedimentary infill of the hangingwall basins in most cases remains inaccessible to direct observation. Furthermore, except for the large Fucino basin (> 1 km depth) that was explored in detail by a grid of seismic commercial profiles (Cavinato et al., 2002; Patacca et al. 2008), most

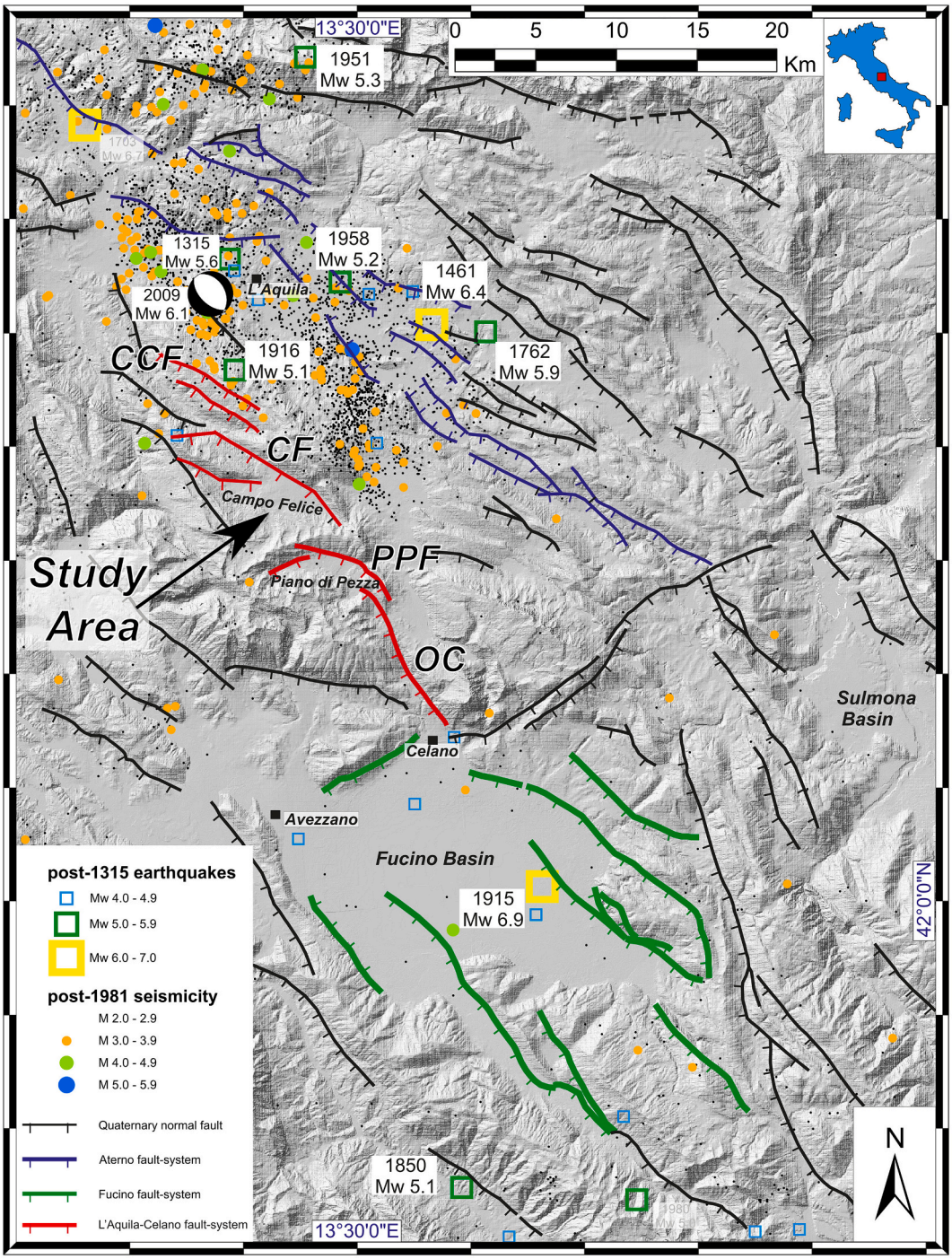

Fig. 1. Seismicity and active normal faults in the central Apennines (modified after Villani et al. 2015). The location of the study area is indicated by the black arrow. Some of the main active normal fault systems are colour-coded: Fucino (green), Middle-Aterno Valley (blue); L'Aquila-Ovindoli-Celano (red). Other fault labels: CF, Campo Felice; CCF, Colle Cerasitto; OC, Ovindoli-Celano; PPF, Piano di Pezza. Instrumental seismicity (small dots) from the Istituto Nazionale di Geofisica e Vulcanologia (INGV) catalog (http://terremoti.ingv.it/). Historical earthquakes (open squares) are from the parametric catalog of Italian historical earthquakes (https://emidius.mi.ingv.it/CPTI/). The focal mechanism of the 2009 L'Aquila earthquake is also shown. (For interpretation of the references to colour in this figure legend, the reader is referred to the web version of this article.)

basins in this region lack a thorough characterization of their subsurface setting (Fig. 1). Therefore, key questions remain often unanswered, particularly those concerning the overall basin geometry and their internal architecture, together with the long-term displacement history of the bounding faults.

In recent years, relevant effort was made to bridge the information gap on the structure of hangingwall basins bounded by the normal faults that ruptured during the M_w 6.1, 2009 L'Aquila earthquake and the M_w 6.5, 2016 Norcia earthquake by shallow geophysical surveys. These studies took their cue from well-established integration of shallow geophysical methods in tectonically active areas (Everett, 2013), including high-resolution active seismics (Morey and Schuster, 1999; Veeken, 2007; Improta and Bruno, 2007, Kaiser et al. 2009; Stephenson et al. 2012, 2013; Osagiede et al. 2014; Gold et al. 2020) and electrical resistivity tomography (ERT; Unsworth et al., 1997; Park and Wernicke, 2003). In particular, seismic profiling and ERT were combined to image the basin interior and fault-zones with decametric to metric spatial resolution (*e.g.*, Villani et al. 2021; Sapia et al. 2021; Bruno et al. 2022;

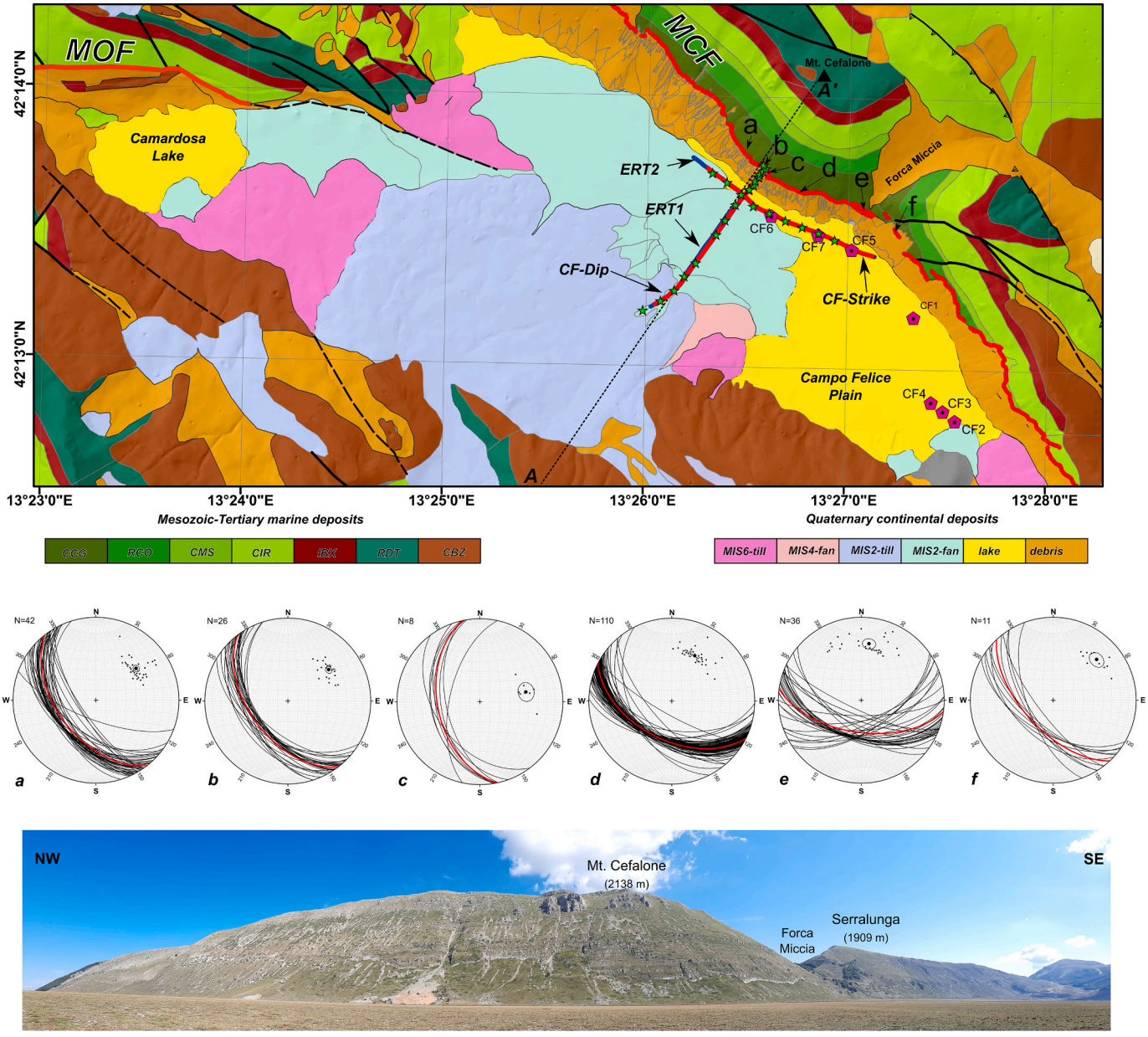

Fig. 2. Geological setting of the Campo Felice basin. The top panel shows the location of the surveys. Red lines: seismic profiles CF-Dip and CF-Strike. Blue lines: ERT profiles 1 and 2. Green stars: continuously recording seismic stations. Pink pentagons: boreholes by Giraudi et al. (2011). Thin black dashed line: trace of geological profile A-A' (see Fig. 12). Thick black lines are normal faults (dashed where inferred), thick red thick lines indicate the main Campo Felice fault system: MCF (Mt. Cefalone fault) and MOF (Mt. Orsello fault). The marine Mesozoic-Cenozoic succession is simplified after Servizio Geologico d'Italia – APAT (2006). Cretaceous marine formations: CCG - Calcari Ciclotemici a Gasteropodi; RCO - Calcari a Requenie; CMS - Calcari e Marne a Carophyta e Salpingoporella Dinarica; IBX - Calcari Intrabauxitici; RDT - Calcari a Radiolitidi. Miocene marine formations: CBZ - Calcari a Briozoi e Litotamni. For the Quaternary continental formations, see details in the text. The mid panel shows original data from our structural surveys performed on 6 different sections of MCF fault (labelled a, b, c, d, e and f). In the stereonets, black small circles indicate fault planes, small black dots poles to the planes, thick black dots mean vector of poles (the small circle indicates the a95 uncertainty cone), and red small circles indicate the attitude of the average fault plane. The bottom panel is a picture of Mt. Cefalone-Mt. Serralunga ridge pointing out the continuous exposure of the MCF fault (Sept. 2021). (For interpretation of the references to colour in this figure legend, the reader is referred to the web version of this article.)

Maraio et al. 2023), illuminating the stratigraphic and structural architecture of these basins, as well as the geometry of subsurface faults and fault-zones properties. Moreover, they helped to better define the fault evolution over the Pleistocene, which in most cases is hardly recognizable from old, low-resolution commercial profiles focused on deep reservoir imaging (see a discussion in: Villani et al. 2021; Bruno et al. 2022).

Following a similar multi-disciplinary approach, in this paper we present the first high-resolution seismic and ERT survey in the Campo Felice basin (central Apennines, Figs. 1 and 2). This basin has been the subject of numerous geological studies, ever since the pioneering work of Bosi (1975), who pointed out the recent activity of the magnificent basin-bounding fault scarp (Mt. Cefalone-Serralunga Fault -MCF; Fig. 1). This fault, exposed for a length of over five kilometers, is part of a major active system, ~30 km-long and defined in the literature as L'Aquila-Ovindoli-Celano (Fig. 1; Salvi and Nardi, 1995; Pantosti et al. 1996; Salvi et al. 2003). The L'Aquila-Ovindoli-Celano fault system is located midway between the seismogenic faults systems of the Middle Aterno Valley (where the source of the 2009 L'Aquila earthquake is located) and the Fucino fault system that ruptured during the Mw 6.9, 1915 Avezzano earthquake. According to seismic rupture scenarios based on fault interaction models (*e.g.*, Mildon et al. 2019), the fault-system bounding Campo Felice basin is a potential candidate for rupturing in the near future with an M 6+ earthquake. This represents a main concern also for the city of Rome, located ~80 km to the south-west, and whose metropolitan area alone has >4.3 million inhabitants (*e.g.*, Ferry et al. 2020; Schirripa Spagnolo et al., 2021).

Most of the previous studies focused on the structural characterization of the main boundary faults (MCF and the adjacent Mt. Orsello Fault –MOF, Fig. 2: Giaccio et al. 2003; Wilkinson et al. 2015; Schirripa Spagnolo et al., 2021; Del Rio et al. 2023). Other studies estimated timing and magnitude of the most recent Holocene seismic cycles of the MCF (*e.g.*, Benedetti et al. 2013; Goodall et al. 2021), thus dealing with a limited span (10^3 a) of the overall fault history (>10^5 a). On the other hand, the basin subsurface was never investigated by geophysical tools: to date, the only information on the sedimentary fill comes from some shallow boreholes (Giraudi et al. 2011; Giraudi and Giaccio, 2017) that do not reach the basin substratum. Consequently, the basin internal structure is unknown and the long-term deformation history of the bounding faults is uncertain.

Our work represents the first contribution to bridge this gap within the Campo Felice basin. We set three main objectives: 1) estimate the basin depth-to-bedrock and infill thickness along a key section orthogonal to the main bounding fault; 2) unravel the nature of the buried sedimentary sequences and their stratigraphic relationships, and define the structural architecture in the central part of the basin; 3) inferring the possible genesis age of the basin, and the relationships between its long-term evolution and fault activity. Although we investigated only the central portion of the basin, this represents a key sector where the largest amount of long-term displacement likely accumulated. Therefore, our study provides a representative picture of the tectonic structure and new valuable information on the bounding normal fault.

2. Geological and structural setting of the Campo Felice Basin

The study area includes two coalescent intramontane depressions standing at an average elevation of 1550–1530 m a.s.l., and extending about 8 km in a NW-SE direction. These depressions (Campo Felice plain s.s. to the east and Camardosa Lake to the west), are located on the hangingwall of two main left-stepping and overlapping SW-dipping normal faults, known as Mt. Cefalone-Serralunga and Mt. Orsello Faults (MCF and MOF in Figs. 1 and 2, respectively). The MCF and MOF fault segments are part of the L'Aquila-Ovindoli-Celano fault-system, a > 30 km-long kinematically coherent fault system with evidence of Holocene activity (*e.g.*, Pantosti et al. 1996; Galli et al. 2008; Villani et al. 2015; Faure Walker et al., 2021). This fault system comprises from the north-west to the south-east: the Colle Cerasitto segment ("CCF" in Fig. 1), the Campo Felice segment ("CF" in Fig. 1, and including the two left-stepping segments MCF and MOF), the Piano di Pezza segment ("PPF" in Fig. 1) and the Ovindoli-Celano segment ("OC" in Fig. 1).

The MCF displays a ~ 5 km-long prominent bedrock fault scarp (Bosi, 1975; Fig. 2), interpreted as mostly due to the coseismic exhumation occurring during discrete slip episodes since the demise of the Last Glacial Maximum (LGM, 19–20 cal ka BP; Clark et al. 2009; Giraudi, 2015). Several studies based on different approaches focused on the estimation of the activity rate of the MCF since the late Pleistocene (*e.g.*, Wilkinson et al. 2015; Goodall et al. 2021), and the quantification of the main coseismic slip phases occurred since the LGM (*e.g.*, Giaccio et al. 2003; Benedetti et al. 2013). For instance, Benedetti et al. (2013) inferred four major earthquakes between 9.4 and 1.1 ka, with an estimated average slip rate in the range of 0.9–2.5 mm/a. These authors also postulated rupture synchrony with the adjacent PPF, where paleoseismic data (Pantosti et al. 1996) suggest two strong (M6.5+) paleoearthquakes occurred ~0.7–1.13 and ~ 5.3–7.0 ka.

In this cross-disciplinary study, we also collected some structural data from the MCF to obtain average strike and dip of the fault that we used for the geological interpretation of our geophysical models. >200 data were collected over six different fault strands close to the seismic profiles based on their average trend (labelled as "a", "b", "c", "d", "e" and "f" from NW to SE; Fig. 1). Results are shown as stereonets in Fig. 2 (top panel). The average strike and dip values for the six fault strands are: a) N142°/052°; b) N143°/052°; c) N168°/048°; d) N117°/052°; e) N098°/058°; f) N137°/061°. The measured dip angle for all strands has an average value of 53.6° ± 6.8°, with higher values (~60°) at the base of the fault scarp, consistent with previous studies (*e.g.*, Wilkinson et al. 2015; Schirripa Spagnolo et al., 2021; Del Rio et al. 2023). Fault kinematics is almost purely dip-slip with mean slip direction ~N206°-210° (*e.g.*, Morewood and Roberts, 2000; Wilkinson et al. 2015).

Both the Campo Felice plain and Camardosa Lake depressions are bounded by limestone ridges made up of over 1 km-thick and generally NE-dipping Jurassic to Late Miocene shallow-water carbonate platform sequence, locally capped by Late Miocene hemipelagic marls and arenaceous turbidites (Fig. 2; Servizio Geologico d'Italia – APAT, 2006).

The Campo Felice plain is ~6 km long and 2.5 km wide. It is filled with a continental succession of lacustrine, glacial till, outwash fan and alluvial deposits from at least the Middle Pleistocene to the Holocene in age (Giraudi, 1995; Giaccio et al. 2003; Giraudi et al. 2011; Fig. 2). In particular, Giraudi and Giaccio (2017) describe seven main sedimentary cycles, due to distinct glacial advances and retreat phases since the Middle Pleistocene, based on the analysis of the drilled nearly continuous lacustrine sequence (indicated with CF1, CF5 and CF7 in Fig. 2). These cycles include alternating clayey silts and rare sandy gravels, where the calcareous silts represent the main product of meltwater from the glaciers during cold periods. The authors correlated those cycles with global marine isotope cold stages (MIS) covering a time span of ~0.5 Ma (from MIS2 to MIS14), thanks to cored tephra that were $^{40}Ar/^{39}Ar$ dated and/or correlated with known eruptions. The following markers are important for our survey: 1) an old tephra (504 ± 9 ka) at a depth of 85 m in borehole CF1; 2) two tephra CF-V11 (457 ± 1.7 ka) and CF-V9 (404 ± 5 ka) found at 107.0 m and 92.4 m depth, respectively, in boreholes CF5–7; 3) tephra CF-V3 (36 ± 1 ka ka cal BP), at ~17 m depth in borehole CF1 and 20 m depth in boreholes CF5–7. A detailed description of the borehole stratigraphy is provided in the Supporting Information (Text S1).

3. Data and methods

3.1. Seismic data acquisition

In 2020, we collected two high-resolution seismic profiles in the central-eastern portion of the Campo Felice basin (labelled as CF-Dip and CF-Strike; Figs. 2 and 3).

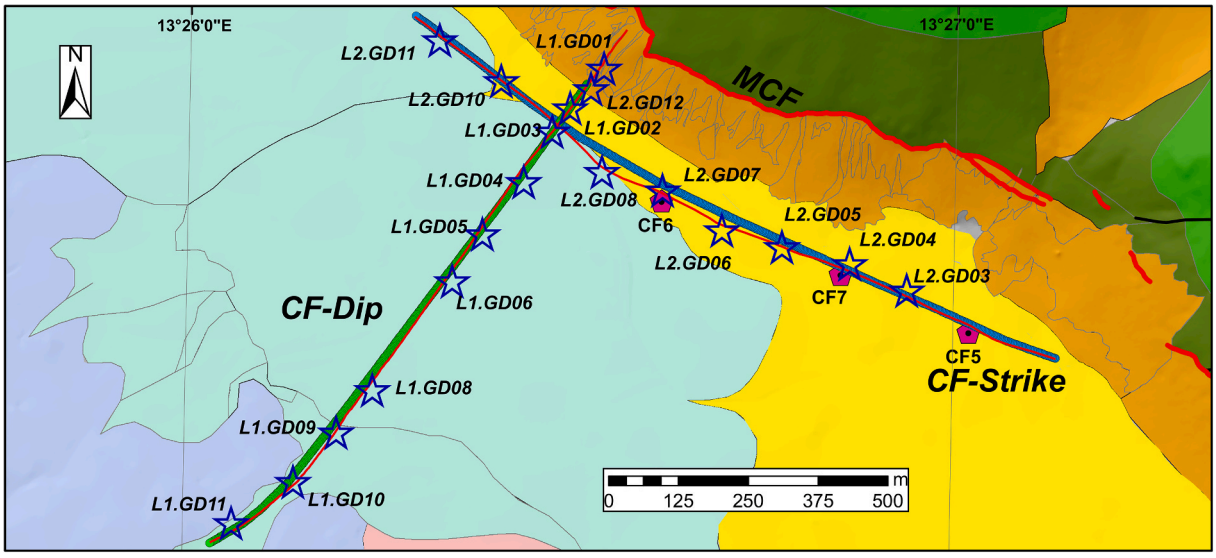

Fig. 3. Geometry of CF-Strike and CF-Dip seismic profiles. The small blue and green circles indicate CMP positions for CF-Strike and CF-Dip, respectively. The thin red lines indicate the true trace of the seismic profiles. The blue stars indicate location of continuously recording seismic stations for microtremor analysis along the two profiles (all results shown in Supporting Information). The pink polygons indicate boreholes. For the meaning of background geology, refer to the caption of Fig. 2. (For interpretation of the references to colour in this figure legend, the reader is referred to the web version of this article.)

They were acquired using a 5455-kg high-frequency vibroseis (MiniVib IVI®: Industrial Vehicles International) that handles a 168 kg mass driven by a hydraulic mechanism. The CF-Dip profile is 1195 m-long and strikes SSW-NNE nearly orthogonal to the average trend of the MCF. It was acquired by deploying an array of 240 vertical geophones (4.5 Hz eigenfrequency), with a spacing of 5 m. The geophones were connected through to 10 multichannel systems (Geode by Geometrics) in serial layout. Its northeast portion is located on a steep debris slope (average surface dip of ~27°), with the extremity ~40 m away from the limestone bedrock outcropping in the MCF footwall.

The location and geometry of this seismic profile was conceived to provide constraints on: 1) the near-fault subsurface sedimentary architecture; 2) the deep geometry of the basin as a response to the long-term activity of the MCF, and interaction with surface processes. The steep slope, unstable debris and the presence of large limestone boulders hampered the use of the vibroseis in the final 235 m of the profile. Here, we were able to fill this gap by using a 5-kg sledgehammer in 74 regularly spaced source points.

The CF-Strike seismic line, located at the piedmont of Mt. Cefalone, is 1315 m-long and nearly parallel to the MCF fault scarp at an average distance of 250–280 m from it. The profile geometry was tied to boreholes CF6, CF5 and CF7 (Fig. 3), which constrain the stratigraphy and the age of the shallow ~100 m of the basin infill. The dataset was acquired deploying an array of 264 vertical geophones (4.5 Hz eigenfrequency), with 5 m spacing.

For both profiles, the source-station spacing was 5 m. At each vibration point, we stacked two 14.4 s long 5–200 Hz upsweeps, with a listening time set to 16 s to record data for a total time of 1.6 s after correlation and a sampling rate of 0.125 ms.

Such a dense wide-aperture acquisition geometry (Bruno et al., 2017, 2022; Improta and Bruno, 2007; Operto et al. 2004) allowed us to obtain high data redundancy (see fold coverage in Fig. S1, Supporting Information) and to collect simultaneously: 1) near-vertical reflections to post-critical wide-angle reflections generated by deep interfaces, and 2) highly redundant first P-pulses corresponding to shallow direct waves, deep penetrating turning waves and critical refractions from the basin interior. This seismic dataset allows combining reflection processing with multi-scale refraction tomography to produce complementary 2D reflection-migrated stack sections and P-wave velocity models.

3.2. Refraction tomography

From the seismic dataset, we hand-picked ~57,000 and 30,000 first-arrival traveltimes for CF-Dip and CF-Strike profiles, respectively (Fig. S2, Supporting Information). They were used to obtain accurate 2-D Vp models through a multi-scale non-linear tomographic inversion (Improta et al. 2002; details in the Supporting Information, Text S2). The multi-scale approach consists in gradually increasing the number of velocity nodes (*i.e.*, the model parameters) during consecutive inversion steps, resulting in an ensemble of models characterized by increasing spatial resolution, achieved at the expense of a loss in resolution depth. Models obtained at intermediate steps of the multi-scale inversion enable the reconstruction of large-scale and deeper velocity structures, while models obtained at late steps provide higher resolution images of the shallow subsurface. To assess resolution of the velocity models, we performed checkerboard tests (details in Text S2). For the models retrieved at an early stage of the multi-scale inversion, the maximum investigation depth inferred by combining back-raytracing plots and checkerboard tests is ~300–400 m (Supporting Information, Figs. S4, S5, S6, S7). For each seismic profile, we show a representative best-fit model resolved down to ~250–350 m that represents a good compromise between the deep and shallow tomographic imaging (Figs. 4a and 6). In this case, the nodes spacing is ~65 m along x and ~ 30 m in depth for CF-Strike (345 parameters; Fig. 4), and ~ 100 m along x and ~ 50 m in depth for CF-Dip (196 parameters; Fig. 6a; details in Text S2). For CF-Dip, we also present a shallower, higher resolution model (200 m-deep) suitable to compare the velocity and resistivity structure in the near-fault subsurface (Fig. 7). This model was obtained by inverting 432 parameters (the node spacing is ~50 m along x and ~ 25 m in depth) and has a resolution depth of 140–180 m.

3.3. Reflection data processing

The reflection processing flow was designed to take advantage of the densely spaced (2.5 m Common Mid Point -CMP spacing) and wide-aperture (maximum offset >1200 m) acquisition geometry. This enables the recording of multi-angle reflections and better focuses the energy reflected from dipping reflectors, such as fault planes and steeply tilted packages expected in the basin subsurface (*e.g.*, Bruno et al. 2019; Maraio et al. 2023). As a first step, we used a pre-processing flow, aimed

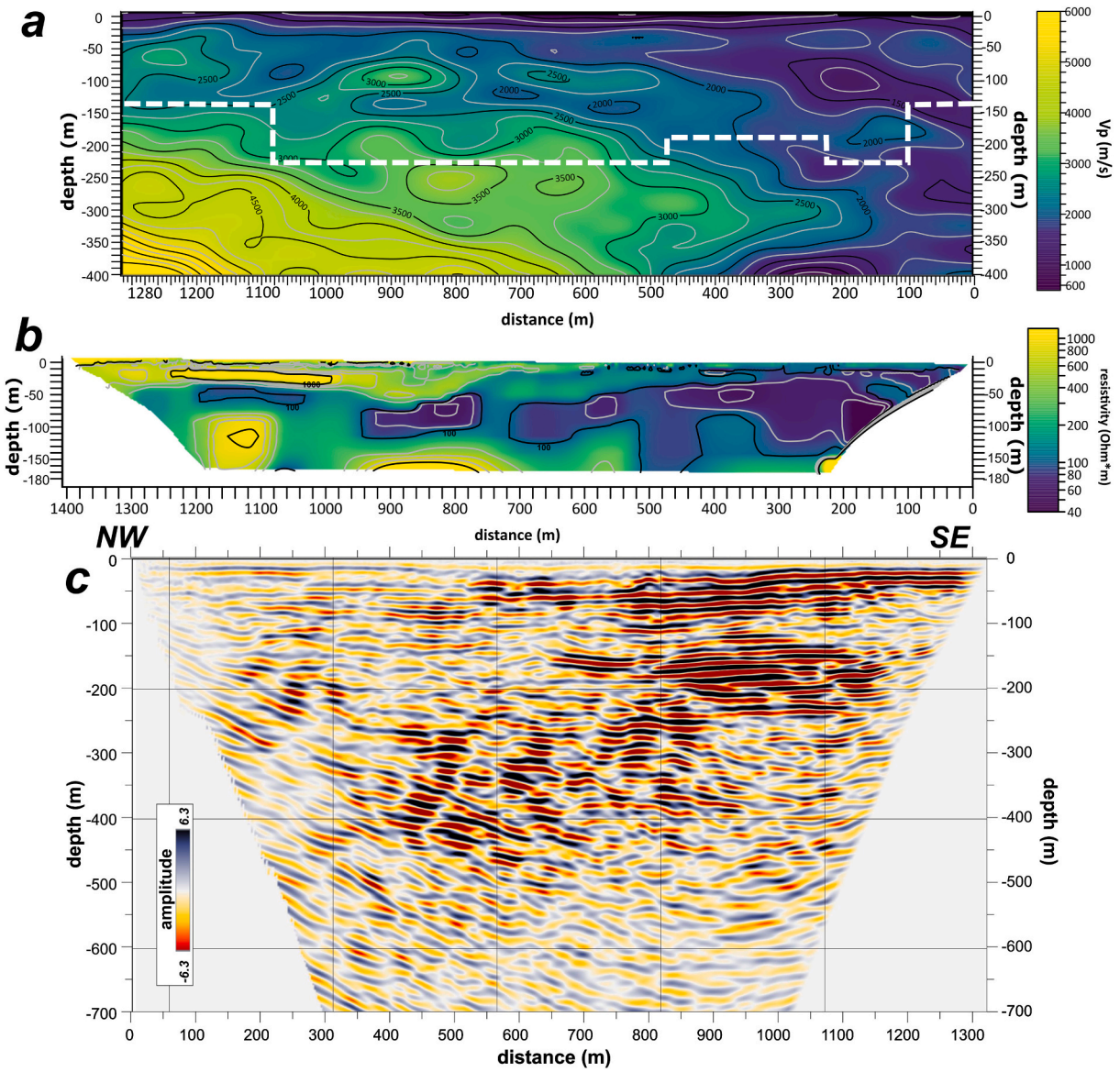

Fig. 4. Results from geophysical investigations along transect CF-Strike. a) Vp tomographic model. The dashed white line shows inferred resolution depth from checkerboard tests (Fig. S7). b) Electrical resistivity model from ERT2 survey. c) Depth-migrated reflection section (datum plane 1540 m a.s.l.).

at improving the signal-to-noise ratio of the data and the resolution of the reflected phases (summarized in Table 1). Then we applied the refraction statics corrections (Taner et al. 1998), using the first arrivals traveltime previously picked from the refraction analysis. The preliminary stack sections were obtained with the standard CMP method, using the root mean square (RMS) velocity models derived from the picking of the semblance functions (Neidell and Taner, 1971). The normal move-out (NMO) velocity models were refined by a cycle of residual statics corrections (Ronen and Claerbout, 1985). For the CF-Dip profile, a dip move-out (DMO) correction (Deregowski, 1986) was applied to the normal move-out corrected prestack data, to preserve conflicting dips (*i.e.*, reflections from the fault plane) with different stacking velocities, then the RMS velocity model was updated based on DMO-corrected CMP gathers and subsequently used for the NMO correction. The stack sections are shown in Fig. S3 (Supporting Information).

Table 1
overview of the pre-processing flow adopted for reflection data.

Processing Step	Details
Trace editing	
True Amplitude Recovery	6 dB/s
AGC	AGC operator length 500 ms
Trace Muting	Top and bottom mute
Surface Consistent Spiking Deconvolution	Operator length 60 ms
Predictive Deconvolution	Operator length 120 ms
Bandpass Filter	10–20–120-150 Hz
Refraction Statics	Final datum 1540 m a.s.l.
Air Blast Attenuation	

In order to create a more accurate image of the subsurface, we applied a Kirchhoff post-stack depth migration on both CF-Dip and CF-Strike stacks. To provide a "background" velocity model for Kirchhoff post-stack migration, we converted the final stacking velocity models in interval velocity vs. depth using the Dix equation (Dix, 1955), employing smoothing functions to the conversion. The depth-migrated sections were finally processed with an F-X deconvolution filter (Gulunay, 1986). Before post-stack depth migration, the spectral resolution (expressed as quarter wavelength $\lambda/4$) for the CF-Dip profile was the following: ~9.2 m (time interval 0–200 ms) and ~ 17.5 m (time-interval 200–500 ms). For the CF-Strike profile, spectral resolution was: ~6.7 m (time-interval

0–300 ms) and ~ 11.7 m (time interval 300–700 ms).

With regard to the CF-Dip profile, we exclusively employed reflection processing on MiniVib-acquired data to ensure uniformity in frequency bandwidth and signal propagation depth. Data collected via hammer source exhibit a very narrow frequency band, rendering them incompatible for joint processing with vibroseis data.

3.4. Electrical resistivity tomography

The seismic investigations were complemented by co-located 2D electrical resistivity tomography (ERT). We acquired a 950 m-long profile using an array of 96 electrodes, 10 m-spaced with the Syscal Pro resistivity meter (powered by IRIS Instruments). Roll-along of 48 electrodes enabled us to cover a maximum length of 1420 m. We adopted both Wenner-Schlumberger and Dipole-Dipole configurations, and the apparent resistivity data were input to a 2D smoothness-constrained least squares inversion algorithm (Constable et al. 1987; Loke and Barker, 1995; Loke and Dahlin, 2002). The quality of the recovered resistivity sections is then described by the RMS of residuals after the last iteration, which is found below 5% after 6 iterations for the two sets of elaborated tomographic models. More details on the technique and data processing are reported in the Supporting Information (Text S6).

3.5. Ambient noise recordings

During the seismic surveys, we deployed 24-bit digitizers (Reftek130) and 5-s 3-component velocimeters (Lennartz LE-3D/5 s) to acquire ambient vibration recordings for a duration ranging from about 2 to 36 h. The stations are located at nearly constant spacing (Fig. 5) of about 150 m along CF-Dip profile (L1.G01 to L1.G12) and about 120 m along CF-Strike profile (L2.G03 to L2.G12). The sampling rate was 250 Hz. Although the seismic stations also recorded the active signals of the MiniVib source (Fig. S8), here the data were analyzed to obtain the Horizontal to Vertical Spectral Ratio (HVSR) function (Molnar et al. 2022), selecting the background seismicity within the quiet period of the experiment. HVSR curves provide the soil resonance frequency peak (F_0), which in the 1D approximation is closely linked to the mean properties (thickness and Vs) of the soft soil over the stiff bedrock (Fäh et al. 2001; Bonnefoy-Claudet et al. 2006). Spectral analysis of waveforms was performed on running time windows of length variable from 30 to 120 s. An anti-trigger algorithm in the time-windows selection was used to suppress spikes and transients. Directional HVSR ratios were also computed (rotating the seismic signal along the horizontal plane using regular bins; Spudich et al., 1996), to investigate the direction (if any) of the predominant polarization of the ground motion. We applied the HVSR technique, as implemented in the Geopsy tool (Wathelet et al. 2020), to try to infer the presence of possible interfaces in the subsurface, and have an independent constraint on the top-to-bedrock depth. We show all the HVSR results along CF-Strike and CF-Dip profiles in the Supporting Information (Fig. S9 and S10; text S4).

4. Results

In this Section, we describe the results of refraction tomography, ERT and reflection processing along the two intersecting transects CF-Strike and CF-Dip, as well as results of the most representative ambient noise recordings collected along the two profiles.

4.1. Profile CF-Strike

The tomographic velocity model (Fig. 4a) shows thick low-Vp deposits (Vp < 2000 m/s) in the southeastern part, down to the resolution depth of 250 m. Here, extremely low-Vp values (< 1250 m/s) prevail in the uppermost 100–120 m. In the central and northwestern portions of the model, the shallow low-Vp layer (< 2000 m/s) grades into a higher velocity region (Vp ~2500–3500 m/s) that also shows velocity reversals. The model hints at a SE-dipping high-Vp region in the lower NW corner (Vp > 3500 m/s) that is poorly resolved because of low ray coverage (Fig. S6, Supporting Information). The co-located ERT model (Fig. 4b) indicates that very-low resistivity (ρ < 50 Ωm) matches the very-low velocity region to the southeast, while relatively high resistivity (ρ ~300–500 Ωm) in the model bottom relates to the region with Vp ~ 3000–3500 m/s in the central deeper part. In the shallower northwestern portion, a high resistivity (ρ > 500 Ωm) layer ~30–50 m thick corresponds to low-velocity near-surface sediments (Vp < 2000 m/s).

The reflection section (Fig. 4c) shows remarkable reflectivity with continuous and high-amplitude reflectors visible down to ~600 m depth. We recognize a shallow portion with continuous reflectors that are nearly horizontal down to depths of ~150 m and ~ 300 m

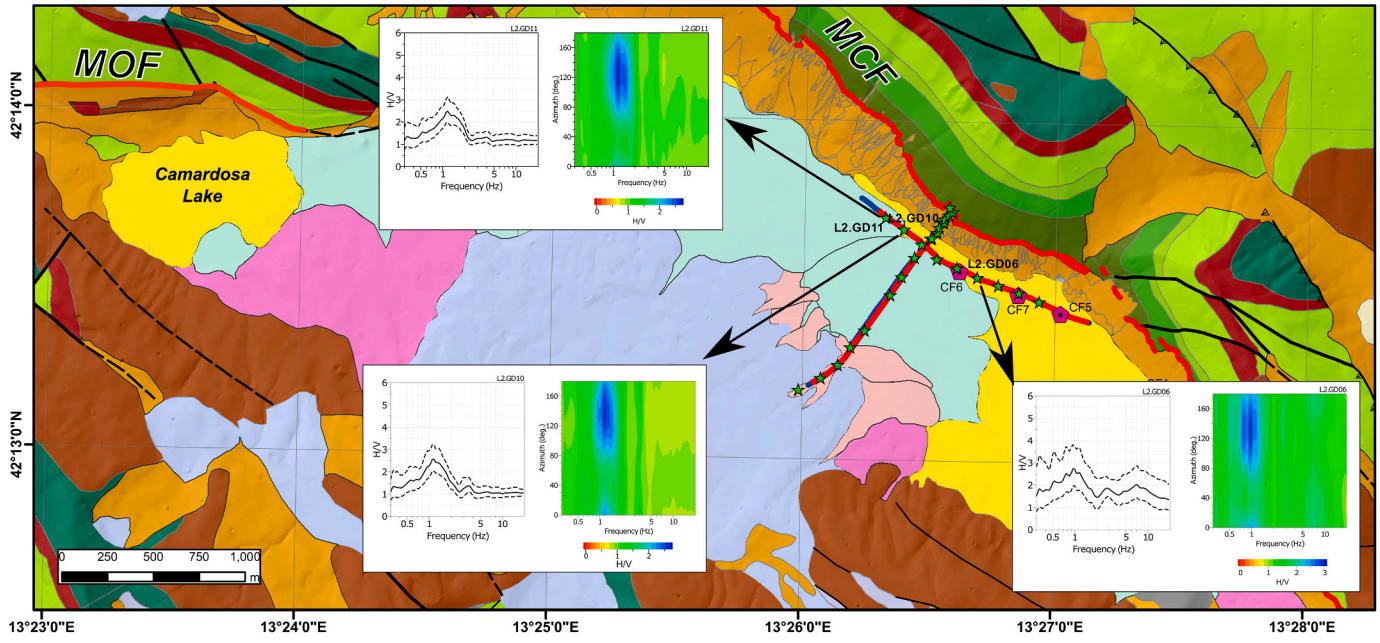

Fig. 5. HVSR analysis for three selected sites along CF-Strike profile. All the results from the collected recordings are shown in Fig. S9 (Supporting Information).

underneath the northwest and southeast parts of the profile, respectively. This reflector configuration indicates the prevalence of thin-bedded sediments. Underneath the southeastern portion of the section, a higher reflectivity suggests alternating fine-grained soils (sands and clays), in agreement with the very-low tomographic velocities and low resistivity values. The upper package of continuous and nearly horizontal reflectors overlies a different sequence that displays less continuous reflectors (at depths ranging from ~250 m to 350 m) with variable and opposing gentle dips, suggesting the local occurrence of cross-bedded coarser deposits. We do not recognize any distinctive channel-like features in the section that might be related to an ancient fluvial system, potentially related to the Forca Miccia wind gap (Fig. 2), as discussed later in Section 5. The whole sequence in the southeastern part of the section attains a maximum thickness of ~450–500 m. These reflectors display an onlap geometry onto SE-dipping high-amplitude events in the northwestern part, thus depicting an unconformity.

The results of passive seismic recordings along CF-Strike are in broad accordance with results of active-source seismic profiling (Fig. 5, Fig. S9 Supporting Information). The HVSR curves show a weak peak (amplitude level < 3 on average) around 1 Hz along the northwestern and central parts of the profile and at lower frequencies (about 0.8 Hz) moving to the southeast. Unfortunately, independent estimates of shear-wave velocities (Vs) are not available, so that the peak of HVSR functions cannot be easily converted to a depth of the main seismic impedance contrast. Additionally, since the proximity of the fault undermines the 1D assumption of these calculations, we use HVSR only to get a crude estimate of the bedrock depth. The Vp tomography model suggests an average Vp of 1900 m/s for the shallow 200 m, decreasing to ~1600 m/s in the southeastern part. Considering a Vp/Vs ratio of ~2.0–2.5 and an f_0 ~ 0.8–1.0 Hz, the resulting depth to the bedrock is in the range of 200–300 m, approximately. The trend of the HVSR peaks is consistent along CF-Strike with a deepening of the basement to the southeast (Fig. 5), paired with a thickening of low-velocity fine-grained soils as shown by active seismic data (Fig. 4). HVSR calculated by rotating the two horizontal components show maximum amplification along a N120° azimuth in correspondence of the resonance peak f_0 (Fig. 5). This direction is roughly parallel to the strike of Mt. Cefalone fault. However, we do not further interpret the fault zone properties since repeated measurements over time would be necessary to confirm the polarization observed during the experiment.

4.2. Profile CF-Dip

The Vp tomographic model (Fig. 6a) has a resolution depth that increases to the north-east, from ~150 m to ~400 m underneath its southern and northern edges, respectively. The shallowest portion of the

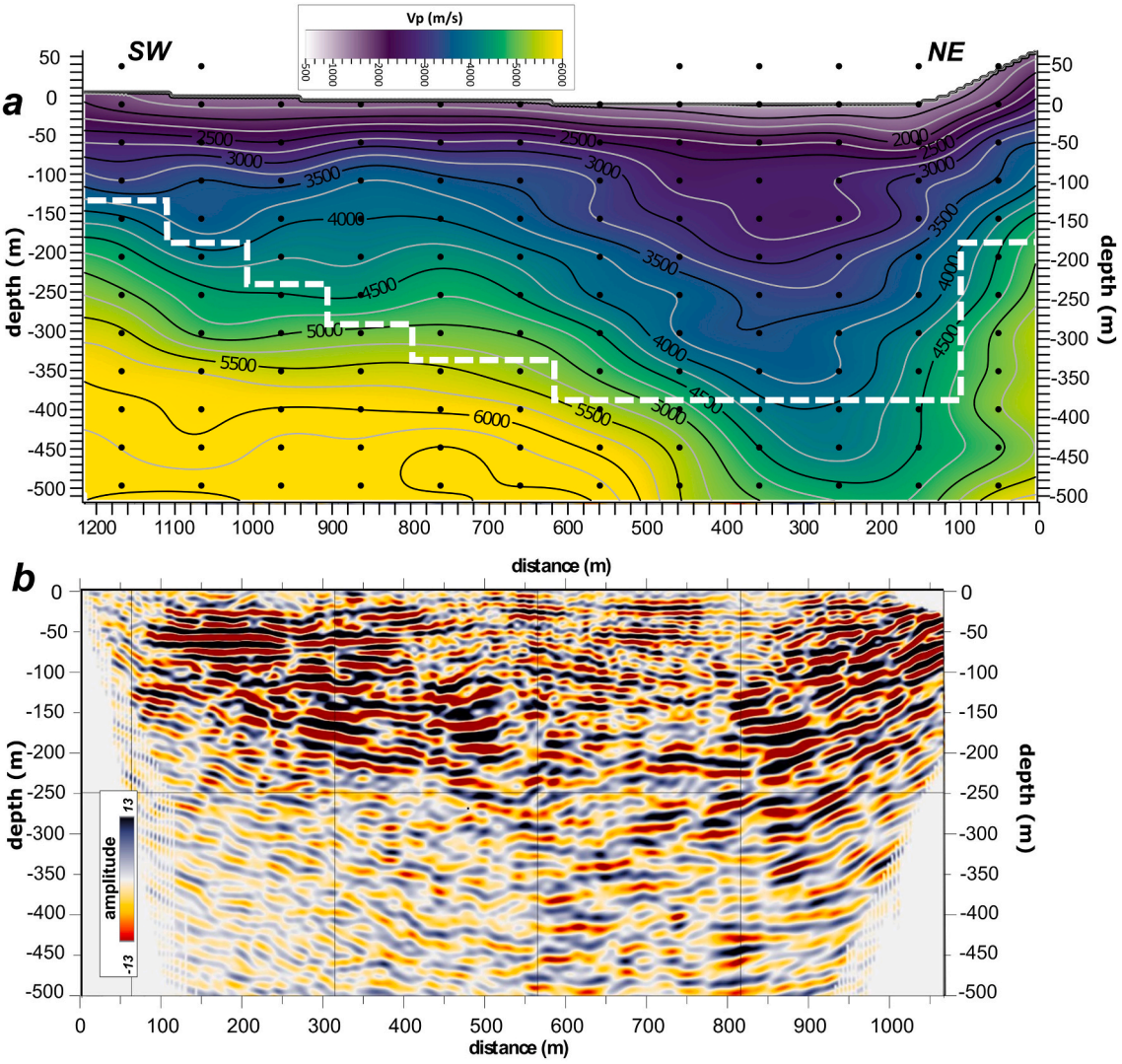

Fig. 6. Seismic investigations along the CF-Dip transect. a) High-resolution tomographic Vp model (345 parameters; nodes spacing: x = 66 m; z = 30 m). The white dashed line shows inferred resolution depth from checkerboard test (Fig. S4, Supporting Information). b) Depth-migrated section.

model (50–80 m depth) is characterized by Vp regularly increasing with depth from 1000 to 2500 m/s. At depths >80 m, the velocity field shows marked lateral variations. In the southwestern part of the model, a shallow (150 m deep) high-Vp body (Vp >4000–4500 m/s) deepens abruptly towards the northeast, reaching over 350 m depth. Above this high-Vp region, an intermediate-Vp region (~2500–3500 m/s) features a wedge-like shape and thickens towards the bounding fault.

The depth-converted migrated reflection section (Fig. 6b) shows clear reflectors down to a depth of ~350 m. The shallow part (0–100 m) features nearly parallel, continuous and high-frequency reflectors displaying a subtle dip to the north-east, in agreement with the Vp tomographic model. In the central part of the section, these events overlie an intermediate sequence of high-amplitude reflectors (100–200 m depth) characterized by a marked dip to the northeast. Close to the northeast edge of the profile, at the base of Mt. Cefalone escarpment, reflectors steeply dip towards the basin interior and show evidence of abrupt truncations. A second zone, which features truncated reflectors and lateral changes in reflector configuration, is located at x = 400–600 m and 150–250 m depth. The bottom of the section displays a lower reflectivity. From seismic tomography, we can associate this deep region of high-Vp (>4000 m/s) with the limestone basement. The lack of large amplitude reflections corresponding to the basement top likely indicates a relatively weak impedance contrast between cemented coarse sediments and limestones, a feature frequently observed in other fault-bounded basins in the Apennines (Villani et al. 2021; Bruno et al. 2022).

The higher-resolution tomographic model in Fig. 7a shows finer details on the low-Vp region close to the base of Mt. Cefalone escarpment. The shallow isovelocity contours gently dip to the northeast, but very-low velocity (Vp <1500 m/s) near-surface sediments thicken in the fault hangingwall. Two strong lateral variations at x ~ 300 m and x ~ 460 m delimit a low-Vp sag (2200–2600 m/s) imaged down to ~200 m depth. Deep lateral Vp changes are also evident at x = 600–800 m. Moreover, the high-Vp region at the northeastern side of the profile is better defined.

The co-located ERT profile (Fig. 7b) images a maximum penetration depth of ~160 m in the central-southern portion. An uppermost near-surface layer of high resistivity (> 1000 Ωm) occurs for mostly the entire section, with thickness decreasing to the northeast from ~100 m to ~50 m. A low-resistivity region (ρ ~200–400 Ωm) generally matches the low-Vp sag developed in the fault hangingwall, while resistivity in the range 600–1000 Ωm characterizes the lower region of high-Vp (> 3000 m/s) under the southwestern part of the transect.

Results from single-station ambient noise recordings along CF-Dip profile are shown in Fig. 8 (all results in Fig. S10, Supporting Information). The HVSR curves do not present a clear low-frequency peak for stations in the southwestern part of the profile. This likely reflects the absence of a strong impedance contrast between the limestone basement and the overlying coarse glacial and alluvial deposits, as previously observed for the velocity models. Moving towards the northeast, at the intersection with profile CF-Strike, HVSR curves show a peak centered at around 1 Hz, consistently with the CF-Dip transect, and with the thickening of the infill wedge of relatively-low velocity sediments (<2400 m/s). In the central sector of the basin and at increasing distances from the CF-Strike profile, directional amplification around N120° azimuth is no longer observed.

5. Interpretation of geophysical investigations along transects CF-Strike and CF-Dip

For the interpretation of the geophysical models, we take into account surface structural data and lithological information from available boreholes (CF5 and CF7, ~100 m-deep; Giraudi et al. 2011), which indicate alternating silty sands and sandy gravels.

Since the CF-Strike profile is nearly parallel to Mt. Cefalone fault, and its horizontal distance from the fault trace ranges from ~250 m (strands "a" and "b" in Fig. 2) to ~280 m (southeastern section, strand "c" in Fig. 2), we expect to see the fault intersection at depth in the migrated reflection section. In fact, by extrapolating straight planes from the outcropping fault surface downwards the predicted fault intersection appears as a low-dip line plunging to the southeast at depths of ~250–450 m (Fig. 9).

Accurate tomographic Vp models of continental basins can yield key information for the geological interpretation of the subsurface, and in particular constrain the lithological interpretation of seismic reflection

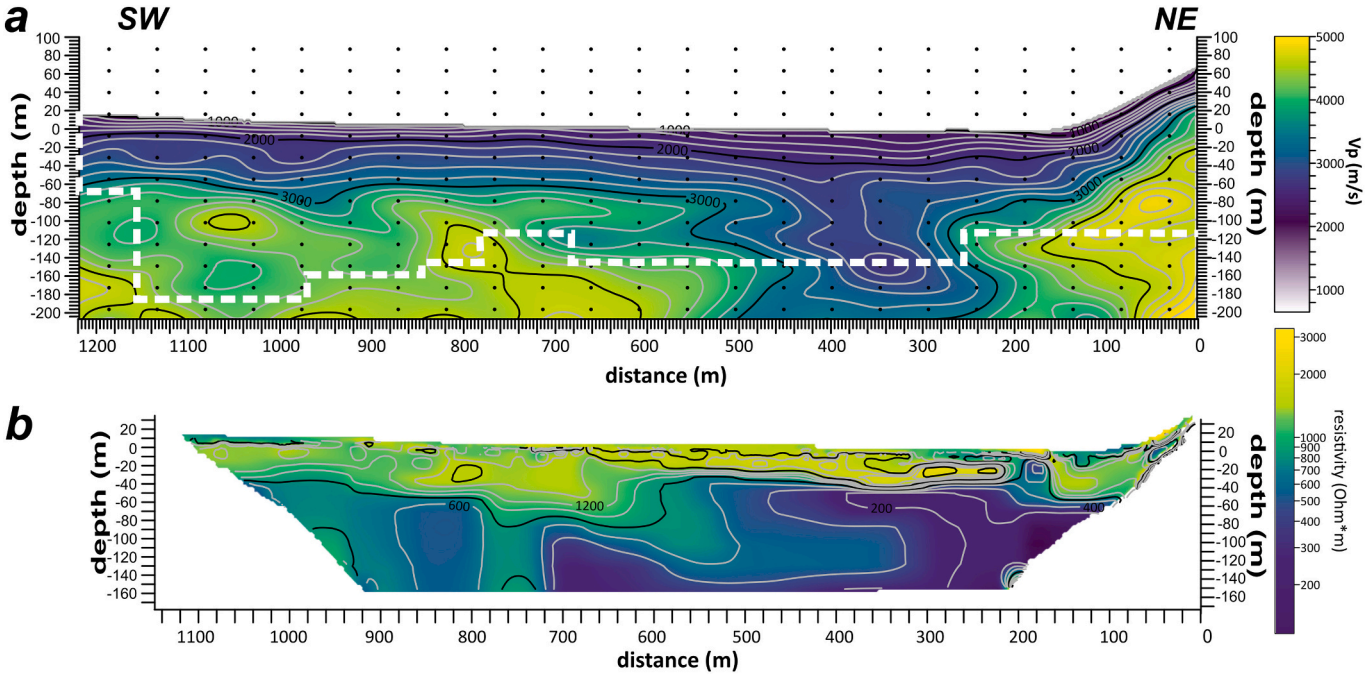

Fig. 7. Comparison of P-wave velocity and resistivity shallow models for profile CF-Dip. a) High-resolution tomographic Vp model (obtained by inverting 432 parameters node spacing ~50 m along x and ~ 25 m in depth). The white line shows resolution depth inferred from checkerboard test (Fig. S5, Supporting Information). b) ERT model (Dipole-Dipole configuration).

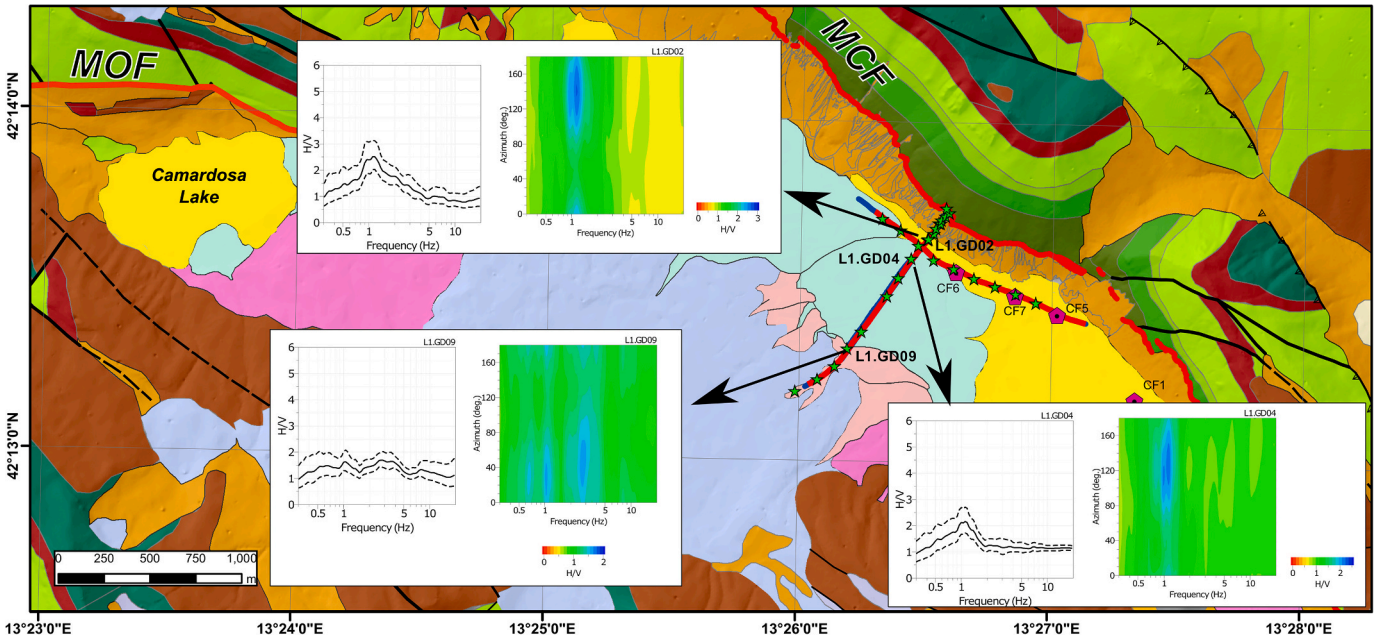

Fig. 8. HVSR analysis for three selected sites along CF-Dip profile. All results from the collected recordings are shown in Fig. S10 (Supporting Information).

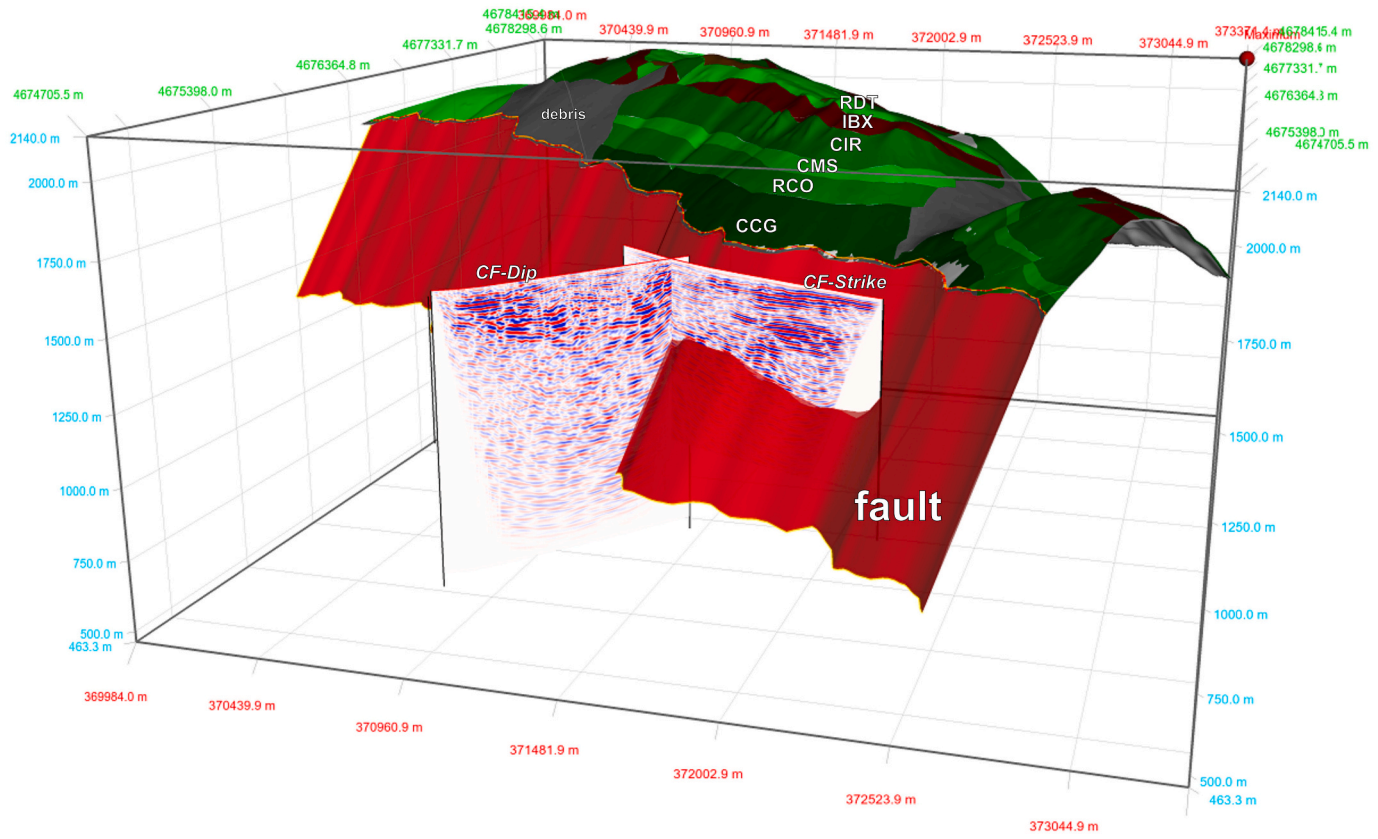

Fig. 9. Predicted geometry of Mt. Cefalone fault at depth and comparison with the location of seismic profiles CF-Dip and CF-Strike. The fault plane extrapolation was done considering an average fault dip of 60° and a simplified fault surface trace (resampling interval of 200 m). The labels of geologic formations are as in Fig. 1. Plot made with the Midland Valley Move Software.

sections in absence of deep calibration wells (see Bruno et al. 2022 among others). Low-Vp regions (Vp < 2000 m/s) can be associated with sandy-silty sediments, whereas relatively higher velocities (Vp > 3000 m/s) are typical of dense and cemented coarse-grained sediments (conglomerates, alluvial fans, breccia, glacial till). The definition of the limestone basement when covered by thick clastic sediments, typical of fault-bounded intramontane Apennines basins, is a major concern. In fact, coarse and high-Vp clastic deposits overlying limestones can

hamper the generation of clear top-bedrock reflections (*e.g.*, Villani et al. 2021; Bruno et al. 2022). In these cases, tomographic velocity models can define the substratum geometry because shallow, fractured limestone feature very-high Vp typically 4000–5000 m/s (*e.g.*, Morandi and Ceragioli, 2002; Latorre et al. 2016 and references therein). Additionally, interpretation must take into account the spatial resolution limits of the migrated stack sections (Text S5, Supporting Information), from which we obtain a theoretical vertical separation limit of ~8–12 m in the shallow part (down to about 250–300 m depth) and of ~12–25 m in the deeper part (below 300 m depth).

Fig. 10 shows a simplified interpretation of the CF-Strike profile. In the southeastern portion, the upper 300 m of the sedimentary infill is interpreted as a sequence of fine-grained deposits related to a lacustrine environment. These layers show a lateral transition to coarse-grained deposits moving to the northwest, likely due to interfingering with slope debris from the Mt. Cefalone escarpment and distal outwash fan gravels fed from the Pleistocene glaciers to the south-west. This is indicated primarily by: 1) the sharp lateral change of electrical resistivity in the shallow ~40–50 m, from >500 Ωm in the northwest to <100 Ωm in the southeast; 2) the change of average Vp in the shallow ~100 m, from ~1550 m/s in the southeastern part to 2200 m/s in the northwest (where the velocity field also shows velocity reversals); 3) the different seismic facies, characterized by uniformly parallel reflections in the southeastern part, and hints of cross-bedding in the northwestern part.

Taking into account information from the tomographic model (Fig. 4a), we suggest that the dipping reflectors found at depths of ~200–500 m are related to coarse sediments with higher velocity (Vp > 2500–3000 m/s) that unconformably overlie a high-Vp (> 4000 m/s) limestone basement. The latter is outlined by continuous and generally high-amplitude reflectors dipping to the southeast. Considering also the predicted intersection of the extrapolated fault plane (Fig. 9), we infer that the top-basement intercepted by the seismic section corresponds to the MCF plane at depth. In fact, the slight obliquity of the average fault trend with respect to the seismic profile results in a line intersection plunging to the southeast. The reflectivity in the limestone basement (at 400–500 m depth) may be due to the following: 1) reverberations generated within the >100 m-wide fault zone (as evidenced by CF-Dip; see next) in a depth interval of ~100 m beneath the fault; 2) reverberations at greater depths. We do not have further data supporting the occurrence of multiples from the well-bedded Cretaceous-Miocene carbonatic platform sequence. At the CF-Dip intersection, the fault plane is inferred at a depth of ~250 m, consistent with the prediction from surface data.

Information provided by key-horizons dated in CF5 and CF7 boreholes (Giraudi et al. 2011; Giraudi and Giaccio, 2017; Section 2) indicates that, the nearly horizontal reflector at 100–110 m depth (marked with a dashed yellow line in Fig. 10) could correspond to a package of sandy layers with an age of ~0.46–0.50 Ma.

A simplified interpretation of the CF-Dip seismic profile is reported in Fig. 11. The shallow layers (0–100 m depth) in the southwestern part correspond to the terminal portion of the glacial till, and the associated outwash fan bodies that prograde towards the east and northeast. This package of reflectors is well-bedded and exhibits a subtle dip towards the Mt. Cefalone fault. Seismic tomography and ERT results (see Fig. 7) indicate that, in the shallow part of this sequence (down to ~60 m depth), relatively high Vp (~2000–3000 m/s) is associated with high resistivity (ρ ~ 800–2000 Ωm), supporting the interpretation of coarse dense deposits with sparse limestone boulders and low matrix content (glacial till), likely featuring a poor water circulation. The deeper part (> 60 m depth) is characterized by relatively lower resistivity values (ρ ~ 400–800 Ωm) and Vp in the 3000–4000 m/s range, suggesting that it likely consists of indurated glacial till and old alluvial deposits. The relatively low resistivity values with respect to the shallow layer can be

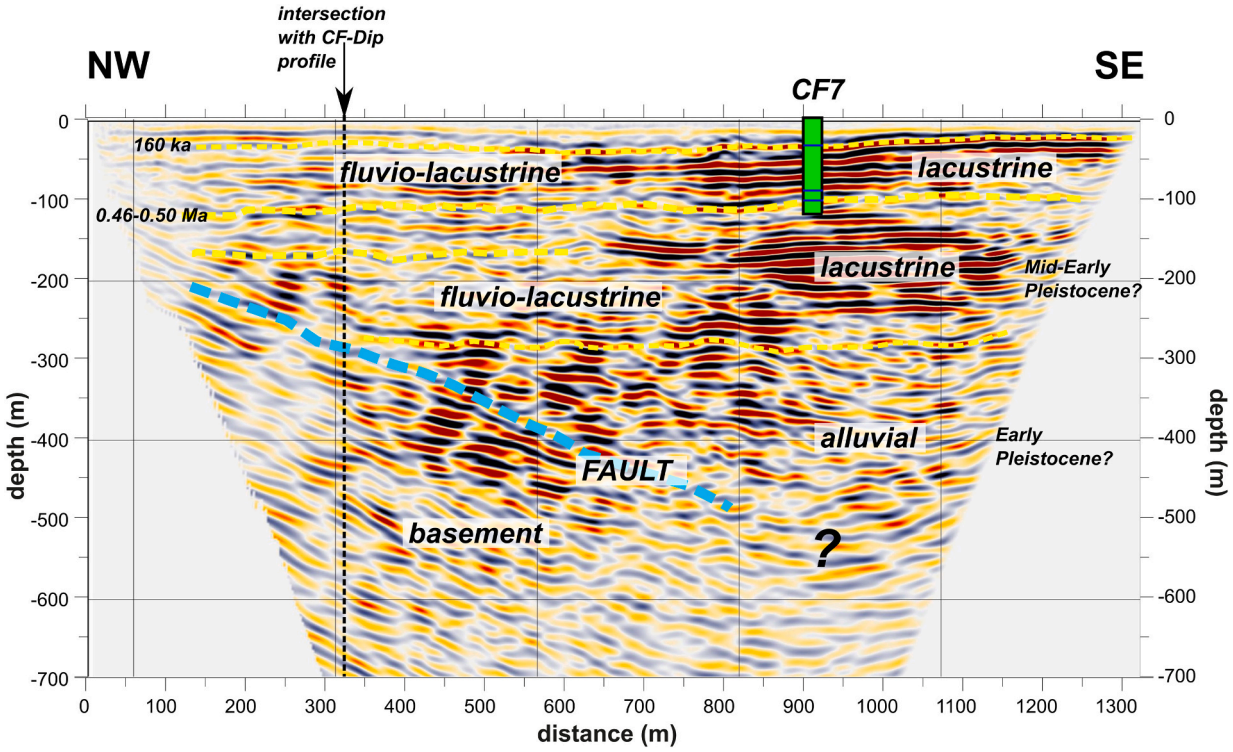

Fig. 10. Simplified geological interpretation of CF Strike reflection profile. The main horizons within the basin infill are marked with yellow dashed lines and the top-bedrock with light blue dashed line. The projected location of borehole CF7 by Giraudi et al. (2011) is shown (thin blue lines indicate only the most important dated horizons). The interpretation of the top-bedrock takes into account the intersection with the Mt. Cefalone fault plane as indicated in Fig. 9. The intersection with the CF-Dip profile is shown with the arrow and the vertical black dashed line. The fault appearing in the seismic section displays an apparent gentle dip to the southeast. (For interpretation of the references to colour in this figure legend, the reader is referred to the web version of this article.)

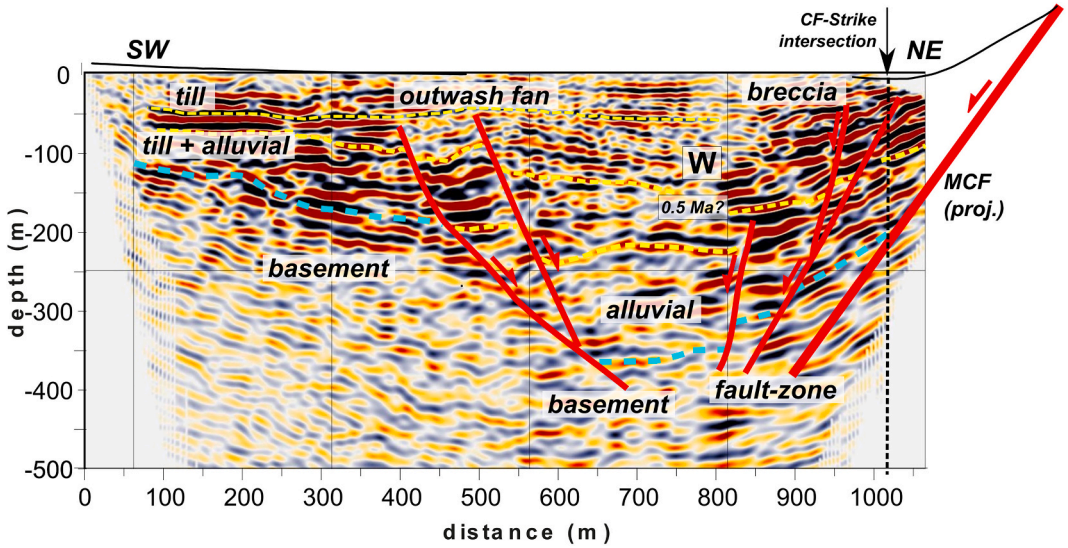

Fig. 11. Simplified interpretation of CF-Dip profile. The main horizons within the infill are marked with dashed yellow lines and the top-bedrock with dashed light blue line. The main faults are in red. The MCF is projected from the outcrop at the surface. The intersection with CF-Strike is shown with the arrow and the vertical black dashed line. The syn-tectonic sedimentary wedge associated with the MCF is outlined by the label "W". (For interpretation of the references to colour in this figure legend, the reader is referred to the web version of this article.)

due to the presence of finer matrix in the alluvial units, possibly combined with a higher water content.

The sequence at ~75–250 m depth in the central and southwestern part of the section shows a more pronounced dip towards the northeast, resulting in a wedge-like body (labelled as "W" in Fig. 11). The latter attests syn-tectonic growth. The seismic facies of the wedge "W", with less continuous and high-amplitude reflectors, together with the associated relatively high Vp values (>3500 m/s), indicate the occurrence of coarse cemented sediments, which we interpret as sequences of alluvial and glacial deposits. The upper part of the wedge (at ~50–100 m depth) is characterized by lower Vp (2200–2600 m/s) and relatively low resistivity (ρ ~200–400 Ωm), indicating finer sediments in the syn-tectonic wedge. Close to the Mt. Cefalone fault, reflectors dipping to the southwest and associated with high Vp (~3000–3500 m/s) can be interpreted as stiff slope breccia, consistent with surface geology (Fig. 2). In this zone, a thin layer that corresponds to a small patch of low resistivity material in the ERT model (x = 220–280 m in Fig. 7b), matches the narrow outcrop of lacustrine sands and silts reported in the geological map (Fig. 2).

In the southwestern part, high-amplitude and gently dipping reflectors at 120–180 m depth match a region of high Vp (>4000 m/s) that we interpret as the response of shallow limestone basement. Taking into account surface geological data, this layer likely corresponds to the marly limestones of the Miocene CBZ Fm., which is >50 m-thick in outcrops in the study area. The integration with tomography also suggests that the maximum depth of the limestone basement is ~350–400 m in the central portion of this transect, although in this part of the section reflections from the carbonate substratum are not clear. We project the Mt. Cefalone fault plane with its average dip (60°) on the section (Fig. 11). The intersection of this plane with profile CF-Strike is at ~250 m depth (considering uncertainty in fault dip at depth), consistent with findings from that profile (see Fig. 10). Therefore, we conclude that the apparent steeply dipping reflectivity matching the fault projection (where tomography indicates Vp ~ 3500–4500 m/s) at 200–400 m depth may be related to reverberations from the Mt. Cefalone fault zone, as seen in profile CF-Strike. We also recognize hints of SW-dipping faults close to the master fault and a couple of closely spaced NE-dipping faults at x = 400–600 m. These latter are delineated by clear reflection truncations and associated reflectors dipping to the southwest. These antithetic faults, which do not seem to deform the sediments shallower than ~50 m, broadly match the deepening of the high-Vp region (Vp > 4000–4500 m/s) in the tomogram (Fig. 6a).

In this interpretation, we extrapolate the information from the intersecting profile CF-Strike, where the tephra markers dated ~0.46–0.50 Ma correspond to a SW-dipping reflector ~110 m-deep located at x = 1000 m. This layer is affected by the SW-dipping fault zone, resulting in a cumulative throw of ~70 m, responsible for the generation of the syn-tectonic wedge "W".

6. Discussion

Different types of extensional basins have been described, based on the spatial arrangement of the largest displacement faults, and the reciprocal relationships between sedimentation/subsidence rates and large-scale vertical movements (*e.g.*, Gawthorpe and Leeder, 2000; Gallen and Wegmann, 2017; Doglioni et al., 1998). When a single bounding normal fault-system dominates, asymmetric large-scale structures develop, commonly known as half-grabens. They are usually bordered by steep escarpments and their typical features are syn-rift infill deposits thickened towards the master fault (Schlische, 1991). Our study shows that the Campo Felice basin can be described as a half-graben with a marked asymmetry of the syntectonic infill, consistent with the early scheme proposed by Bosi (1975) and published geological sections based on field surface data (see Section 2). Compared to previous models (*e.g.*, Schirripa Spagnolo et al. 2021; Del Rio et al. 2023), the novelty of our study lies in providing the first geophysical constraints to the reconstruction of the basin structure. This gives new information on the long-term activity of the basin-bounding fault.

6.1. Structural and sedimentary architecture of the Campo Felice basin

Our seismic images, combined with electrical resistivity models, document that the sedimentary infill of Campo Felice basin is ~350–400 m-thick along the CF-Dip transect and likely >500 m along the CF-Strike transect. The continental infill is very heterogeneous, including sequences of coarse-grained (fluvio-glacial, glacial and alluvial) and fine-grained (distal alluvial and lacustrine) deposits that display lateral gradational changes.

Seismic profile CF-Strike is nearly parallel to the Mt. Cefalone fault. The imaged shallow layers (down to ~300 m depth) of the depositional

sequence are nearly sub-horizontal, suggesting that the pattern of tectonic subsidence is rather constant along the profile. Scientific drillings located along the southeastern side of the profile (Giraudi et al. 2011) penetrated the upper ~110 m of the stratigraphic sequence, which is made of alternating lacustrine clays and sandy gravels that contribute to a marked reflectivity. These layers show very-low Vp values (~1250–2000 m/s) and very-low resistivity ($\rho < 50$ Ωm) that enable extending the interpretation of the fine-grained and clay-rich lacustrine facies, down to a conservative depth of ~250–300 m under the eastern part of the profile. Notably, the ~460 ka marker set at 107 m depth in boreholes CF5 and CF7 puts an important constraint on timing of sedimentation and deformation in the basin. We found that the thickness of the lacustrine succession is at least three times greater than previously inferred from borehole data alone (see for instance the structural scheme reported in Fig. 3 of Giraudi et al. 2011). Assuming realistic sedimentation rates prior to the deposition of the ~0.46–0.50 Ma levels (0.2–0.5 mm/a within internally drained tectonic basins in the central Apennines; *e.g.*, Giaccio et al. 2019), this implies a noticeable persistence of the lake environment in this sector of the basin due to fault-driven internal drainage. Therefore, the oldest continental deposits trapped in the hangingwall volume reasonably date back to the Early Pleistocene (> 1 Ma).

The deeper part of the sedimentary succession recognizable in the Campo Felice basin can be ascribable to an alluvial cycle up to ~200 m-thick. This interpretation is based on the comparison of tomographic velocities (Vp ~ 2500–3500 m/s) with seismic facies (*i.e.*, high amplitude, low-frequency and less continuous reflectors, locally displaying evidence of cross-bedding; Fig. 10). We consider the alternative interpretation in terms of Miocene flysch unlikely. In fact, Cenozoic terrigenous rocks outcrop only outside the basin area to the east of Mt. Serralunga ridge (Fig. 2), while the seismic facies of these deeper layers do not resemble that typical of deformed Miocene synorogenic deposits.

One possible interpretation is that this deep alluvial cycle can be related to a previous phase of exorheic drainage (*e.g.*, Bosi, 1975; Giraudi and Frezzotti, 1997; Giraudi et al. 2011), attested by the occurrence of a wind gap on Mt. Cefalone ridge (Forca Miccia in Fig. 2). Concerning this old alluvial cycle, from the CF-Strike profile we do not see in the continental infill any evidence of channel structures clearly constraining paleo-drainage across the Mt. Cefalone-Serralunga ridge (Fig. 10). Rather, the interpreted deep alluvial layers exhibit an apparent dip that matches with the underlying limestone basement dipping to the southeast. If any form of palaeo-drainage orthogonal to the fault ever existed, we suspect it must be older, even predating the deposition of the oldest infill deposits visible in the seismic section. Although our geophysical data are not conclusive concerning previous outflow conditions in the Campo Felice basin, they suggest an older inception of faulting and a longer duration of internal drainage conditions than previously assumed (*e.g.*, Lanari et al. 2021).

CF-Dip profile (Fig. 11) is orthogonal to the average trend of Mt. Cefalone fault. In this section, the seismic facies of shallow layers and surface geological data (Fig. 2) indicate that the infill material is mostly made of coarse glacial till interfingering with outwash alluvial fan deposits, mixed with slope breccia close to the base of Mt. Cefalone escarpment. The thickness of the glacial deposits (>50 m) is larger than any outcrop in the basin: this is indicative of the occurrence of different stacked sequences of glacial deposits. The fan deposits are well organized in parallel and continuous reflectors with generally high amplitude, indicative of alternating sands and gravels characterized by high impedance contrast. Their attitude describes a wedge due to syn-sedimentary faulting.

By extrapolating the ~0.46–0.50 Ma markers onto profile CF-Dip from the intersecting CF-Strike profile, we infer that the shallow 75–100 m of the glacial sequence were deposited since the MIS14 (dated ~0.56 Ma). The alluvial sequence in the fault hangingwall deepens due to fault back-tilt down to ~130–150 m b.g.l. Taking into account these depth and age values, we obtain a near-fault sedimentation rate of ~0.26–0.32 mm/a, which becomes ~0.20–0.22 mm/a along profile CF-Strike, located ~250–280 m from the surface fault trace. The sedimentary sequence of coarse deposits, of probable glacial origin, deepens down to ~250–275 m depth along profile CF-Dip.

The MCF is associated with two blind antithetic faults (at x = 450–600 m along profile CF-Dip) that were unknown prior to our survey. This fault architecture is in agreement with the structural setting of other extensional basins in the central Apennines investigated by seismic profiling and other geophysical techniques; L'Aquila basin (Improta et al. 2012; Villani et al. 2017; Bruno et al. 2022), Castelluccio di Norcia basin (Villani et al. 2019, 2021; Ercoli et al. 2020); Norcia basin (Ercoli et al. 2020), San Demetrio basin (Pucci et al. 2016; Civico et al. 2017), Gubbio basin (Collettini et al. 2003). The key role of antithetic faults in accommodating extensional deformation is also documented by the recent normal-faulting M6+ sequences of the central Apennines featuring multi-segment rupture processes (Valoroso et al. 2013; Improta et al. 2019; Tan et al. 2021).

The antithetic faults give rise to the relatively narrow shape of the Campo Felice basin, compared to the overall master fault dimensions. If we rule out the occurrence of recent sub-seismic displacements, the significant activity of these faults likely ceased before the sedimentation of the outwash package ~50 m-thick, in the final part of the Middle Pleistocene.

6.2. *Hints on the long-term displacement and slip-rates of Mt. Cefalone fault*

We can evaluate from CF-Dip a minimum cumulative geologic throw of the Mt. Cefalone fault based on the geological section (Fig. 12). Given the absence of deep calibration wells, the proposed reconstruction of the top-basement geometry is an attempt that could be improved with further surveys (including new drillings and additional seismic profiling). Moreover, we do not have any constraint on the amount of erosion affecting the Meso-Cenozoic succession. In the geological section, we chose a configuration of the top-basement that roughly follows the stratigraphic boundary between RDT Fm. (Cretaceous) and CBZ Fm. (Miocene), which are nearly para-concordant (Servizio Geologico d'Italia-APAT, 2006; Fig. 2). Our conservative estimate of the maximum total fault throw is ~1200 m with a downdip displacement of ~1500 m. This transect is parallel and close to geological profiles L-L' by Schirripa Spagnolo et al. (2021; see their Fig. 5 reporting a maximum throw of 1480 m) and A-A' by Del Rio et al. (Del Rio et al. 2023; see their Fig. 2 reporting a maximum throw of 1050 m).

In terms of overall geometry, the model in Fig. 12 is in general agreement with previous ones based on field geology. Compared to the results by Schirripa Spagnolo et al. (2021), our displacement estimate is lower, because seismic images support a shallower dip of the basement underneath the sediment cover. We also note that the thickness of the infill material is <30% of the total geological throw, as found in other fault-bounded extensional basins in the Apennines (*e.g.*, Bonini et al. 2019; Buttinelli et al. 2021). Although the continental succession should contain hiatuses due to pauses in sedimentation and erosional phases, results from CF-Strike profile suggest a prolonged persistence of the lacustrine environment (Section 6.1). Therefore, internally drained conditions may have preserved a large fraction of the syn-rift sedimentary record in the Campo Felice basin.

In addition, our data provide information on the Quaternary kinematic evolution.

So far, published slip-rates for the MCF span a relatively short time interval (approximately since the end of the LGM), and are in the 0.8–2.5 mm/a range (Section 2). Computing slip-rates of the MCF on longer timescales is hindered by the lack of information on the age of the continental infill at depths >100 m. Moreover, due to the lack of correlative Quaternary layers in the footwall of the MCF, a precise calculation of the Quaternary slip is not possible. Here are just a few pointers that may help reduce slip-rate uncertainties.

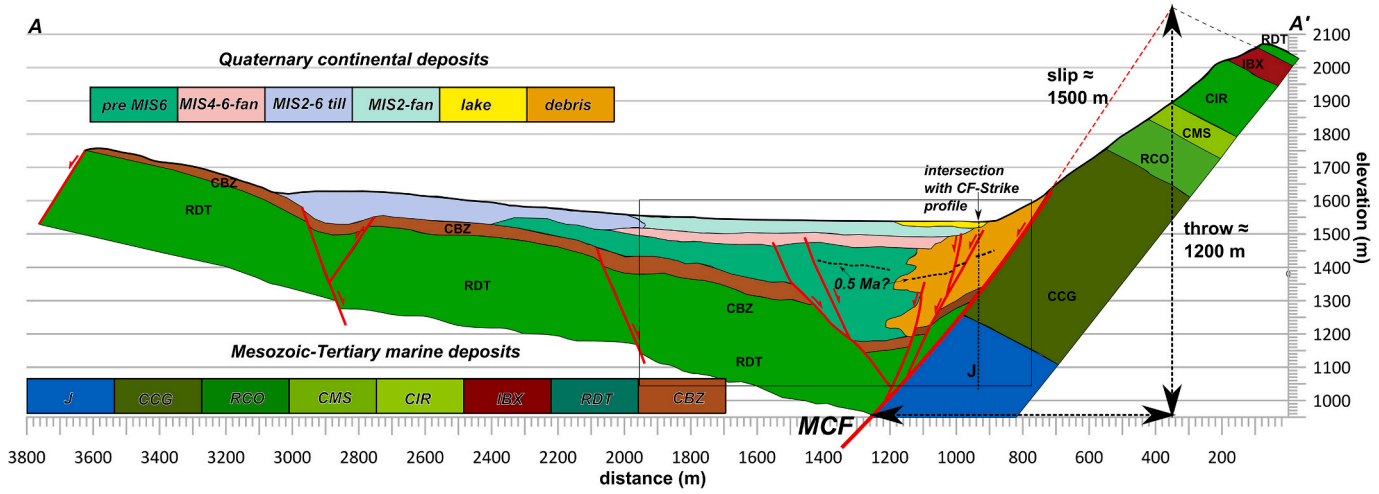

Fig. 12. Interpreted geological cross-section along CF-Dip profile (trace A-A' in Fig. 2). The small black rectangle indicates the area constrained by seismic data. For the meaning of labels, refer to the caption of Fig. 2 (J represents undifferentiated Jurassic units below the CCG Fm.). The pre-MIS7 layer is an undifferentiated alluvial unit, possibly containing older unknown fluvio-lacustrine and glacial deposits, heteropic with slope breccia.

The tephra CF-V11 (457 ± 1.7 ka) found at 107.0 m depth is a benchmark that we can follow along the CF-Strike profile and by correlation along part of the CF-Dip profile. Being located ~250 m from the outcropping MCF, it can be used as a marker of cumulative near-fault displacement occurring in the past ~0.5 Ma. We infer that the post-0.5 Ma slip on the MCF may be ~100–250 m, obtained by restoring the ~0.5 Ma layers faulted by secondary splays (~70–80 m of throw; Fig. 11) and assuming that subsidence was only due to fault displacement (which we cannot prove with our available data). These values represent a minimum for the post-0.5 Ma displacement of the MCF, and imply a long-term (10^5 a) slip-rate of ~0.2–0.5 mm/a. Since published structural data (*e.g.*, Morewood and Roberts, 2000) indicate a dominant dip-slip kinematics with some local oblique component observed only close to the southeastern fault tip (Wilkinson et al. 2015), we think that any possible component of transtensional deformation little affect the estimation of the dip slip-rate.

Our results suggest that higher slip-rates, as those inferred since the LGM (Section 2), are not compatible with the geometry of the deeper sequences imaged by our seismic profiles. In fact, the ~0.5 Ma marker would have had to be at a greater depth in the near-fault. Such a discrepancy between short-term and long-term slip-rates would deserve further investigation supported by new subsurface data and dated cores collected throughout the area.

7. Conclusions

Our geophysical investigations provide the first subsurface images of the Campo Felice basin, a fault-bounded intramontane depression in the Apennines seismic belt. This basin is bounded by a system of SW-dipping active normal faults showing hints of large (*e.g.*, M6+) surface-rupturing paleoearthquakes and representing a high priority seismogenic source for earthquake research, due to its relatively small distance (~80 km) from the metropolitan area of Rome (> 4.3 million inhabitants).

We focused on two transects parallel (CF-Strike) and orthogonal (CF-Dip) to the main bounding fault (Mt. Cefalone-Serralunga fault, MCF), by acquiring high-resolution seismic data collected with a multi-fold wide-aperture geometry, electrical resistivity profiles, and ambient noise recordings.

The integration of geophysical models proved crucial to shed light on the basin internal architecture due to the presence of a heterogenous infill consisting of sequences of fine-grained and coarse-grained continental deposits that display lateral gradational changes. The basin structure is further complicated by blind antithetic and synthetic fault splays that were unknown prior to our study. By a methodological point of view, our results confirm once more that the combination of different geophysical imaging techniques with field geological surveys is fundamental to investigate complex continental tectonic basins, especially where the lack of deep calibration wells hinder complete structural and stratigraphic interpretation of seismic reflection profiles.

Our data define the Campo Felice basin as an asymmetric half-graben filled with a wedge-like syn-tectonic sedimentary sequence thickening towards the master fault. The maximum thickness is approximately 350–400 m along profile CF-Dip and likely >500 m along profile CF-Strike. The lithology of the infill material is constrained by scientific drilling in the uppermost ~100 m of the sequence, and it mainly consists of clayey-silts and sandy-silts in the southeastern part (displaying Vp < 2000 m/s and resistivity $\rho < 100$ Ωm), and coarse-grained sediments in the northern part (displaying Vp > 2500–3000 m/s and resistivity $\rho >$ 500 Ωm). Our results unravel a long-lived lacustrine environment in the southeastern portion of the basin, where it is filled by fine-grained, conductive and low-Vp sediments ~250–300 m thick at least. From borehole data, the shallow ~100 m of the infill deposited in the past ~0.5 Ma. This implies a long-term sedimentation rate ~ 0.2 mm/a, from which we speculate that the age of the deeper part of the sedimentary infill, made of lacustrine and alluvial cycles, spans the whole Middle Pleistocene and probably also part of the Early Pleistocene.

The seismic profile CF-Dip unravels the shallow structure of the MCF, with a fault zone at least 200 m wide, which includes several splays covered by alluvial and debris deposits. We estimate that along the investigated transect the MCF accrued a total displacement of ~1500 m with a throw of ~1200 m. From the configuration of reflectors and associated dated horizons, the inferred minimum displacement accrued by the MCF in the past ~0.5 Ma was ~100–250 m. These findings have two main consequences. First, considering that the maximum thickness of sediment hosted in the hangingwall is ~500 m, this may indicate that a significant fraction of the geologic displacement was accrued before the beginning of sedimentation in the basin, possibly in the Early Pleistocene. Second, we obtain a post-0.50 Ma slip-rate of ~0.20–0.50 mm/a along the investigated transect, lower than the post-LGM slip rates published so far (~1 mm/a).

Understanding the age of basin inception and clarifying the timing of fault activity will be the focus of our next research. In this view, our first images of the basin subsurface and the recognition of a thick fine-grained lacustrine sequence provide key information for future scientific drilling projects.

CRediT authorship contribution statement

F. Villani: Writing – original draft, Visualization, Validation, Methodology, Investigation, Formal analysis, Data curation, Conceptualization. **S. Maraio:** Writing – review & editing, Visualization, Methodology, Investigation, Formal analysis, Data curation. **L. Improta:** Writing – review & editing, Validation, Supervision, Resources, Project administration, Methodology, Investigation, Funding acquisition, Conceptualization. **V. Sapia:** Writing – review & editing, Visualization, Methodology, Investigation, Formal analysis, Data curation. **G. Di Giulio:** Writing – review & editing, Visualization, Investigation, Formal analysis, Data curation. **P. Baccheschi:** Writing – review & editing, Validation, Investigation, Data curation. **M. Pischiutta:** Writing – review & editing, Validation, Investigation, Formal analysis, Data curation. **M. Vassallo:** Writing – review & editing, Investigation, Formal analysis, Data curation. **V. Materni:** Writing – review & editing, Investigation. **P.P. Bruno:** Writing – review & editing, Validation, Investigation. **C.A. Brunori:** Writing – review & editing, Investigation. **R. Civico:** Writing – review & editing, Investigation. **A. D'Alessandro:** Writing – review & editing, Investigation. **C. Felicetta:** Writing – review & editing, Investigation. **S. Lovati:** Writing – review & editing, Investigation. **T. Ricci:** Writing – review & editing, Investigation. **S. Scudero:** Writing – review & editing, Investigation. **P.M. De Martini:** Writing – review & editing, Validation, Supervision, Resources, Project administration, Methodology, Investigation, Funding acquisition.

Declaration of Competing Interest

The authors declare that they have no known competing financial interests or personal relationships that could have appeared to influence the work reported in this paper.

Data availability

Data will be made available on request.

Acknowledgements

This work has been funded by the Istituto Nazionale di Geofisica e Vulcanologia (INGV) Project "Pianeta Dinamico 2020-2022" (code CUP D53J19000170001) funded by the Italian Ministry of University and Research "Fondo finalizzato al rilancio degli investimenti delle amministrazioni centrali dello Stato e allo sviluppo del Paese, legge 145/2018" under an agreement between INGV and Centro di Geotecnologie (CGT) of Siena University (activities performed in the framework of Task S2 "*Struttura 3D dell'Italia da analisi multidato. Sismica passiva/attiva, Prospezioni magnetiche, magnetotelluriche, elettriche, gravimetriche*" WP2, Coordinator Luigi Improta). We warmly thank Mariantonietta Brancale, Lisa Serri, Alessio Lorenzetti and Paolo Manganello for their support in the field. We also thank the mayor of Lucoli (Mr. Walter Chiappini), the Carabinieri Forestali of Tornimparte, the A.N.A.S. Regione Abruzzo and the Sirente-Velino Regional Park that provided the authorizations for performing the geophysical surveys in Campo Felice.

We greatly appreciated two anonymous reviewers for their constructive comments that helped us improve our manuscript. Francesco Emanuele Maesano and Mauro Buttinelli are thanked for fruitful discussions on the kinematic analysis of the surveyed fault structure. Carlo Doglioni is thanked for his encouragement and support that made this and other active seismic experiments possible.

We acknowledge support of this work via a Landmark Grant Program to INGV by Halliburton Software and Services, a Halliburton Company.

Many thanks to the "ESITO" INGV Laboratory (https://www.ingv.it/monitoraggio-e-infrastrutture/laboratori/laboratorio-effetti-di-sito) for kindly providing us part of the seismic instrumentation used in this work. We acknowledge support of the INGV's Reflection Seismology Laboratory "SismoLab-3D" (https://sismolab3d.ingv.it/) for the Midland Valley Move software.

Appendix A. Supplementary data

Supplementary data to this article can be found online at https://doi.org/10.1016/j.tecto.2023.230170.

References

Benedetti, L., Manighetti, I., Gaudemer, Y., Finkel, R., Malavieille, J., Pou, K., Arnold, M., Aumaître, G., Bourlès, D., Keddadouche, K., 2013. Earthquake synchrony and clustering on Fucino faults (Central Italy) as revealed from in situ 36Cl exposure dating. J. Geophys. Res. Solid Earth 118, 4948–4974. https://doi.org/10.1002/jgrb.50299.

Boncio, P., Lavecchia, G., Pace, B., 2004. Defining a model of 3D seismogenic sources for Seismic Hazard Assessment applications: The case of central Apennines (Italy). J. Seismol. 8, 407–425. https://doi.org/10.1023/B:JOSE.0000038449.78801.05.

Bonini, L., Basili, R., Burrato, P., Cannelli, V., Fracassi, U., Maesano, F.E., et al., 2019. Testing different tectonic models for the source of the Mw 6.5, 30 October 2016, Norcia earthquake (Central Italy): a youthful normal fault, or negative inversion of an old thrust? Tectonics 38, 990–1017. https://doi.org/10.1029/2018TC005185.

Bonnefoy-Claudet, S., Cecile, C., Pierre-Yves, B., Fabrice, C., Peter, M., Jozef, K., Fäh, D., 2006. H/V ratio: a tool for site effects evaluation. Results from 1-D noise simulations. Geophys. J. Int. 167 (2), 827–837.

Bosi, C., 1975. Osservazioni preliminari su faglie probabilmente attive nell'Appennino centrale. Ital. J. Geosci. 94 (4), 827–859.

Bruno, P.P.G., Maraio, S., Festa, G., 2017. The shallow structure of Solfatara Volcano, Italy, revealed by dense, wide-aperture seismic profiling. Sci. Rep. 7 (1), 17386. https://doi.org/10.1038/S51598-017-17589-3.

Bruno, P.P.G., Berti, C., Pazzaglia, F.J., 2019. Accommodation, slip inversion and segmentation in a province-scale shear zone from high-resolution, densely spaced, wide-aperture seismic profiling, Centennial Valley, MT, USA. Sci. Rep. 9, 9214. https://doi.org/10.1038/S51598-019-45497-1.

Bruno, P.P., Villani, F., Improta, L., 2022. High-resolution seismic imaging of fault-controlled basins: a case study from the 2009 Mw 6.1 L'Aquila Central Italy earthquake. Tectonics 41. https://doi.org/10.1029/2022TC007207 e2022TC007207.

Bull, W.B., 2009. Tectonically active Landscapes. Wiley. https://doi.org/10.1002/9781444312003.

Burbank, D.W., Anderson, R.S., 2011. Tectonic Geomorphology, 2nd edition. Wiley-Blackwell. https://doi.org/10.1002/9781444345063.

Buttinelli, M., Petracchini, L., Maesano, F.E., D'Ambrogi, C., Scrocca, D., Marino, M., et al., 2021. The impact of structural complexity, fault segmentation and reactivation on seismotectonics: Constraints from the upper crust of the 2016-2017 Central Italy seismic sequence area. Tectonophysics 810, 228861. https://doi.org/10.1016/j.tecto.2021.228861.

Cavinato, G.P., Carusi, C., Dall'Asta, M., Miccadei, E., Piacentini, T., 2002. Sedimentary and tectonic evolution of Plio–Pleistocene alluvial and lacustrine deposits of Fucino Basin (central Italy). Sediment. Geol. 148 (1–2), 29–59. https://doi.org/10.1016/S0037-0738(01)00209-3.

Chiarabba, C., Buttinelli, M., Cattaneo, M., De Gori, P., 2020. Large earthquakes driven by fluid overpressure: the Apennines normal faulting system case. Tectonics 39. https://doi.org/10.1029/2019TC006014 e2019TC006014.

Civico, R., Sapia, V., Di Giulio, G., Villani, F., Pucci, S., Baccheschi, P., Amoroso, S., Cantore, L., Di Naccio, D., Hailemikael, S., Smedile, A., Vassallo, M., Marchetti, M., Pantosti, D., 2017. Geometry and evolution of a fault-controlled Quaternary basin by means of TDEM and single-station ambient vibration surveys: the example of the 2009 L'Aquila earthquake area. J. Geophys. Res. https://doi.org/10.1002/2016JB013451.

Clark, P.U., Dyke, A.S., Shakun, J.D., Carlson, A.E., Clark, J., Wohlfarth, B., Mitrovica, J. X., Hostetler, S.W., McCabe, A.M., 2009. The last Glacial Maximum. Science 325 (5941), 710–714. https://doi.org/10.1126/science.1172873.

Collettini, C., Barchi, M.R., Chiaraluce, L., Mirabella, F., Pucci, S., 2003. The Gubbio fault: can different methods give pictures of the same object? J. Geodyn. 36, 51–66. https://doi.org/10.1016/S0264-3707(03)00038-3.

Constable, S.C., Parker, R.L., Constable, C.G., 1987. Occam's inversion: a practical algorithm for generating smooth models from electromagnetic sounding data. Geophysics 52 (3). https://doi.org/10.1190/1.1442303.

Cosentino, D., Asti, R., Nocentini, M., Gliozzi, E., Kotsakis, T., Mattei, M., Esu, E., Spadi, M., Tallini, M., Cifelli, F., Pennacchioni, M., Cavuoto, G., Di Fiore, V., 2017. New insights into the onset and evolution of the central Apennine extensional intermontane basins based on the tectonically active L'Aquila Basin (central Italy). Geol. Soc. Am. Bull. 129 (9/10), 1314–1336.

Cowie, P.A., Roberts, G.P., 2001. Constraining slip rates and spacings for active normal faults. J. Struct. Geol. ISSN: 0191-8141 23 (12), 1901–1915.

Cowie, P., Phillips, R., Roberts, G., et al., 2017. Orogen-scale uplift in the central Italian Apennines drives episodic behaviour of earthquake faults. Sci Rep 7, 44858. https://doi.org/10.1038/srep44858.

D'Agostino, N., Mantenuto, S., D'Anastasio, E., Giuliani, R., Mattone, M., Calcaterra, S., Gambino, P., Bonci, L., 2011. Evidence for localized active extension in the central Apennines (Italy) from global positioning system observations. Geology 39, 291–294. https://doi.org/10.1130/G31796.1.

Del Rio, L., Moro, M., Masoch, S., Fawzi, D., Saroli, M., Cavallo, A., Di Toro, G., 2023. Architecture of active extensional faults in carbonates: Campo Felice and Monte D'Ocre faults, Italian Apennines. Journal of Structural Geology 169. https://doi.org/10.1016/j.jsg.2023.104828.

Deregowski, S.M., 1986. What is DMO? First Break 4, 7–24. https://doi.org/10.3997/1365- 2397.1986014.

Dix, C.H., 1955. Seismic velocities from surface measurements. Geophysics 20 (1), 68–86. https://doi.org/10.1190/1.1438126.

Doglioni, C., D'Agostino, N., Mariotti, G., 1998. Normal faulting vs regional subsidence and sedimentation rate. Mar. Petrol. Geol. 15 (8), 737–750. https://doi.org/10.1016/S0264-8172(98)00052-X.

Ercoli, M., Forte, E., Porreca, M., Carbonell, R., Pauselli, C., Minelli, G., Barchi, M.R., 2020. Using seismic attributes in seismotectonic research: an application to the Norcia Mw = 6.5 earthquake (30 October 2016) in Central Italy. Solid Earth 11, 329–348. https://doi.org/10.5194/se-11-329-2020.

Fäh, D., Kind, F., Giardini, D., 2001. A theoretical investigation of average h/v ratios. Geophys. J. Int. 145, 535–549. https://doi.org/10.1046/j.0956-540x.2001.01406.x.

Ferry, M., Gautier, S., Mazzotti, S., Villani, F., Stell, E., Jacottin, M., Pantosti, D., Sapia, V., Ricci, T., Benedetti, L., Di Giulio, G., Vassallo, M., 2020. Structure and Segmentation of the Ovindoli – Piano di Pezza – Campo Felice Fault System (Central Apennines, Italy): Evolution and Reactivation of Inherited Faults, EGU General Assembly 2020, Online, 4–8 May 2020, EGU2020–7362. https://doi.org/10.5194/egusphere-egu2020-7362.

Galadini, F., Galli, P., 2000. Active tectonics in the central Apennines (Italy) - input data for seismic hazard assessment. Nat. Hazards 22, 225–268. https://doi.org/10.1023/A:1008149531980.

Gallen, S.F., Wegmann, K.W., 2017. River profile response to normal fault growth and linkage: an example from the Hellenic forearc of south-central Crete, Greece. Earth Surf. Dynam. 5, 161–186. https://doi.org/10.5194/esurf-5-161-2017.

Galli, P., Galadini, F., Pantosti, D., 2008. Twenty years of paleoseismology in Italy. Earth Sci. Rev. 88 (1), 89–117. https://doi.org/10.1016/j.earscirev.2008.01.001.

Gawthorpe, R.L., Leeder, M.R., 2000. Tectono-sedimentary evolution of active extensional basins. Basin Research 12, 195–218. https://doi.org/10.1111/j.1365-2117.2000.00121.x.

Geurts, A.H., Cowie, P.A., Duclaux, G., et al., 2018. Drainage integration and sediment dispersal in active continental rifts: A numerical modelling study of the central Italian Apennines. Basin Res 30, 965–989. https://doi.org/10.1111/bre.12289.

Ghisetti, F., Vezzani, L., 1999. Depth and modes of Pliocene–Pleistocene crustal extension of the Apennines (Italy). Terra Nova 11, 67–72. https://doi.org/10.1046/j.1365-3121.1999.00227.x.

Giaccio, B., Galadini, F., Sposato, A., Messina, P., Moro, M., Zreda, M., et al., 2003. Image processing and roughness analysis of exposed bedrock fault planes as a tool for paleoseismological analysis: results from the Campo Felice fault (central Apennines, Italy). Geomorphology 49 (3–4), 281–301. https://doi.org/10.1016/S0169-555X(02)00191-5.

Giaccio, B., Leicher, N., Mannella, G., Monaco, L., Regattieri, R., Wagner, B., et al., 2019. Extending the tephra and palaeoenvironmental record of the Central Mediterranean back to 430 ka: a new core from Fucino Basin, Central Italy. Quat. Sci. Rev. 225, 106003 https://doi.org/10.1016/j.quascirev.2019.106003.

Giraudi, C., 1995. Considerations on the significance of some postglacial fault scarps in the Abruzzo Apennines (Central Italy). Quat. Int. 25, 33–45. https://doi.org/10.1016/1040-6182(94)00033-2.

Giraudi, C., 2015. The upper Pleistocene deglaciation on the Apennines (peninsular Italy). Cuadernos de investigación geográfica 41 (2), 337–358. https://doi.org/10.18172/cig.2696.

Giraudi, C., Frezzotti, M., 1997. Late Pleistocene Glacial events in the Central Apennines, Italy. Quatern. Res. 48 (3) https://doi.org/10.1006/qres.1997.1928.

Giraudi, C., Giaccio, B., 2017. Middle Pleistocene glaciations in the Apennines, Italy: new chronological data and preservation of the glacial record. Geol. Soc. Lond. Spec. Publ. 433 (1), 161–178. https://doi.org/10.1144/SP433.1.

Giraudi, C., Bodrato, G., Lucchi, M.R., Cipriani, N., Villa, I.M., Giaccio, B., Zuppi, G.M., 2011. Middle and late Pleistocene glaciations in the Campo Felice Basin (central Apennines, Italy). Quatern. Res. 75 (1), 219–230. https://doi.org/10.1016/j.yqres.2010.06.006.

Gold, R.D., Stephenson, W.J., Briggs, R.W., DuRoss, C.B., Kirby, E., Woolery, E., et al., 2020. Seismic reflection imaging of the low-angle Panamint normal fault system, eastern California. Journal of Geophysical Research: Solid. Earth 125 (11). https://doi.org/10.1029/2020JB020243 e2020JB020243.

Goodall, H.J., Gregory, L.C., Wedmore, L.N.J., McCaffrey, K.J.W., Amey, R.M.J., Roberts, G.P., et al., 2021. Determining histories of slip on normal faults with bedrock scarps using cosmogenic nuclide exposure data. Tectonics 40. https://doi.org/10.1029/2020TC006457 e2020TC006457.

Gulunay, N. 1986. FXDECON and complex wiener prediction filter. *SEG Technical Program Expanded Abstracts,*279-281. https://doi.org/10.1190/1.1893128.

Improta, L., Bruno, P.P., 2007. Combining seismic reflection with multifold wide aperture profiling: an effective strategy for high-resolution shallow imaging of active faults. Geophys. Res. Lett. 34, L20310. https://doi.org/10.1029/2007GL031893.

Improta, L., Zollo, A., Herrero, A., Frattini, M., Virieux, J., Dell'Aversana, P., 2002. Seismic imaging of complex structures by non-linear traveltime inversion of dense wide-angle data: Application to a thrust belt. Geophys. J. Int. 151, 264–278. https://doi.org/10.1046/j.1365-246X.2002.01768.x.

Improta, L., Villani, F., Bruno, P.P., Castiello, A., De Rosa, D., Varriale, F., Punzo, M., Brunori, C.A., Civico, R., Pierdominici, S., Berlusconi, A., Giacomuzzi, G., 2012. High-resolution controlled-source seismic tomography across the Middle Aterno basin in the epicentral area of the 2009, Mw 6.3, L'Aquila earthquake (central Apennines, Italy). Italian. J. Geosci. 131 (3), 373–388. https://doi.org/10.3301/IJG.2011.35.

Improta, L., Latorre, D., Margheriti, L., Nardi, A., Marchetti, A., Lombardi, A.M., et al., 2019. Multi-segment rupture of the 2016 Amatrice- Visso-Norcia seismic sequence (Central Italy) constrained by the first high-quality catalog of early aftershocks. Sci. Rep. 9, 6921. https://doi.org/10.1038/S51598-019-43393-2.

Kaiser, A.E., Green, A.G., Campbell, F.M., Horstmeyer, H., Manukyan, E., Langridge, R. M., McClymont, A.F., Mancktelow, N., Finnemore, M., Nobes, D.C., 2009. Ultrahigh-resolution seismic reflection imaging of the Alpine Fault, New Zealand. J. Geophys. Res. 114, B11306. https://doi.org/10.1029/2009JB006338.

Lanari, R., Faccenna, C., Benedetti, L., Sembroni, A., Bellier, O., Menichelli, I., et al., 2021. Formation and persistence of extensional internally drained basins: the case of the Fucino basin (Central Apennines, Italy). Tectonics 40. https://doi.org/10.1029/2020TC006442 e2020TC006442.

Latorre, D., Mirabella, F., Chiaraluce, L., Trippetta, F., Lomax, A., 2016. Assessment of earthquake locations in 3-D deterministic velocity models: a case study from the Altotiberina near fault observatory (Italy). J. Geophys. Res. Solid Earth 121, 8113–8135. https://doi.org/10.1002/2016JB013170.

Loke, M.H., Barker, R.D., 1995. Least-square inversion of apparent resistivity pseudosections. Geophysics 60, 1682–1690. https://doi.org/10.1190/1.1443900.

Loke, M.H., Dahlin, T., 2002. A comparison of the Gauss-Newton and quasi-Newton methods in resistivity imaging inversion. J. Appl. Geophys. 49, 149–162. https://doi.org/10.1016/S0926-9851(01)00106-9.

Maraio, S., Villani, F., Bruno, P.P., Sapia, V., Improta, L., 2023. Active fault detection and characterization by ultrashallow seismic imaging: a case study from the 2016 Mw 6.5 Central Italy earthquake. Tectonophysics. https://doi.org/10.1016/j.tecto.2023.229733.

Mildon, Z.K., Roberts, G.P., Faure Walker, J.P., et al., 2019. Coulomb pre-stress and fault bends are ignored yet vital factors for earthquake triggering and hazard. Nat. Commun. 10, 2744. https://doi.org/10.1038/S51467-019-10520-6.

Molnar, S., Sirohey, A., Assaf, J., Bard, P.Y., Castellaro, S., Cornou, C., Cox, B., Guillier, B., Hassani, B., Kawase, H., Matsushima, S., 2022. A review of the microtremor horizontal-to-vertical spectral ratio (MHVSR) method. J. Seismol. 26 (4), 653–685. https://doi.org/10.1007/s10950-021-10062-9.

Morandi, S., Ceragioli, E., 2002. Integrated interpretation of seismic and resistivity images across the "Val d'Agri" graben (Italy). Ann. Geophys. 45, 259–271. https://doi.org/10.4401/ag-3510.

Morewood, N.C., Roberts, G.P., 2000. The geometry, kinematics and rates of deformation within an en échelon normal fault segment boundary, Central Italy. J. Struct. Geol. 22 (8), 1027–1047. https://doi.org/10.1016/S0191-8141(00)00030-4.

Morey, D., Schuster, G.T., 1999. Paleoseismicity of the Oquirrh fault, Utah from shallow seismic tomography. Geophys. J. Int. 138 (1), 25–35. https://doi.org/10.1046/j.1365-246x.1999.00814.x.

Neidell, N.S., Taner, M.T., 1971. Semblance and other coherency measures for multichannel data. Geophysics 36 (3), 482–497. https://doi.org/10.1190/1.1440186.

Nicol, A., Walsh, J.J., Villamor, P., Seebeck, H., Berryman, K.R., 2010. Normal fault interactions, paleoearthquakes and growth in an active rift. J. Struct. Geol. 32 (8), 1101–1113. https://doi.org/10.1016/j.jsg.2010.06.018.

Nixon, C.W., Bull, J.M., Sanderson, D.J., 2014. Localized vs distributed deformation associated with the linkage history of an active normal fault, Whakatane Graben, New Zealand. J. Struct. Geol. 69, 266–280.

Operto, S., Ravaut, C., Improta, L., Virieux, J., Herrero, A., Dell'Aversana, P., 2004. Quantitative imaging of complex structures from dense wide-aperture seismic data by multiscale traveltime and waveform inversions: a case study. Geophys. Prospect. 52, 625–651. https://doi.org/10.1111/j.1365-2478.2004.00452.x.

Osagiede, E.E., Duffy, O.B., Jackson, C.A.-L., Wrona, T., 2014. Quantifying the growth history of seismically imaged normal faults. Journal of Structural Geology 66, 382–399. https://doi.org/10.1016/j.jsg.2014.05.021.

Pantosti, D., D'Addezio, G., Cinti, F.R., 1996. Paleoseismicity of the Ovindoli-Pezza fault, central Apennines, Italy: a history including a large, previously unrecorded earthquake in the Middle Ages (860–1300 a.D.). J. Geophys. Res. 101 (B3), 5937–5959. https://doi.org/10.1029/95JB03213.

Park, S.K., Wernicke, B., 2003. Electrical conductivity images of Quaternary faults and Tertiary detachments in the California Basin and Range. Tectonics 22 (4). https://doi.org/10.1029/2001TC001324.

Patacca, E., Scandone, P., Di Luzio, E., Cavinato, G.P., Parotto, M., 2008. Structural architecture of the central Apennines: Interpretation of the CROP 11 seismic profile from the Adriatic coast to the orographic divide. Tectonics 27, TC3006. https://doi.org/10.1029/2005TC001917.

Pucci, S., Civico, R., Villani, F., Ricci, T., Delcher, E., Finizola, A., Sapia, V., De Martini, P.M., Pantosti, D., Barde-Cabusson, S., Brothelande, E., Gusset, R., Mezon, C., Orefice, S., Peltier, A., Poret, M., Torres, L., Suski, B., 2016. Deep Electrical Resistivity Tomography along the tectonically active Middle Aterno Valley (2009 L'Aquila earthquake area, Central Italy). Geophys. J. Int. https://doi.org/10.1093/gji/ggw308.

Ronen, J., Claerbout, J.F., 1985. Surface-consistent residual statics estimation by stack-power maximization. Geophysics 50 (12), 2759–2767. https://doi.org/10.1190/1.1441896.

Salvi, S., Cinti, F., Colini, L., D'addezio, G., Doumaz, F., Pettinelli, E., 2003. Investigation of the active Celano–L'Aquila fault system, Abruzzi (central Apennines, Italy) with combined ground-penetrating radar and palaeoseismic trenching. Geophys. J. Int. 155 (3), 805–818. https://doi.org/10.1111/j.1365-246X.2003.02078.x.

Salvi, S., Nardi, A., 1995. The Ovindoli Fault: a segment of a longer, active fault zone in central Abruzzi, Italy, in *Perspectives in Paleoseismology*, Vol. 6, pp. 101-113, (Eds.) Serva, L. and Slemmons, D.B., Bull. Assoc. Eng. Geol.

Sapia, V., Villani, F., Fischanger, F., Lupi, M., Baccheschi, P., Pantosti, D., et al., 2021. 3-D deep electrical resistivity tomography of the major basin related to the 2016 Mw 6.5 Central Italy earthquake fault. Tectonics 40. https://doi.org/10.1029/2020TC006628 e2020TC006628.

Schirripa Spagnolo, G., Mercuri, M., Billi, A., Carminati, E., Galli, P., 2021. The segmented Campo Felice normal faults: Seismic potential appraisal by application of empirical relationships between rupture length and earthquake magnitude in the central Apennines, Italy. Tectonics 40. https://doi.org/10.1029/2020TC006465 e2020TC006465.

Schlische, R.W., 1991. Half-graben basin filling models: new constraints on continental extensional basin development. Basin Res. 3 (3), 123–141. https://doi.org/10.1111/j.1365-2117.1991.tb00123.x.

Servizio Geologico d'Italia-APAT, 2006. Foglio 359 "L'Aquila" della Carta Geologica d'Italia alla scala 1:50,000. http://www.isprambiente.gov.it/Media/carg/359_LAQUILA/Foglio.html.

Serpelloni, E., Cavaliere, A., Martelli, L., Pintori, F., Anderlini, L., Borghi, A., et al. (2022). Surface Velocities and Strain-Rates in the Euro-Mediterranean Region From Massive GPS Data Processing. *Front. Earth Sci.*, 01 June 2022, Sec. Solid Earth Geophysics, 10-2022. https://doi.org/10.3389/feart.2022.907897.

Stephenson, W.J., Odum, J.K., Williams, R.A., McBride, J.H., Tomlison, I., 2012. Characterization of intrabasin faulting and deformation for earthquake hazards in Southern Utah Valley, Utah, from high-resolution seismic imaging. Bull. Seismol. Soc. Am. 102 (2), 524–540. https://doi.org/10.1785/0120110053.

Spudich, P., Hellweg, M., Lee, H.K., 1996. Directional topographic site response at Tarzana observed in aftershocks of the 1994 Northridge, California, earthquake: Implications for mainshock motions. Bull. Seismol. Soc. Am. 86, S193–S208.

Stephenson, W.J., Frary, R.N., Louie, J., Odum, J.K., 2013. Quaternary extensional growth folding beneath Reno, Nevada, imaged by urban seismic profiling. Bull. Seismol. Soc. Am. 103 (5), 2921–2927. https://doi.org/10.1785/0120120311.

Tan, Y.J., Waldhauser, F., Ellsworth, W.L., Zhang, M., Zhu, W., Michele, M., et al., 2021. Machine-learning-based high-resolution earthquake catalog reveals how complex fault structures were activated during the 2016–2017 Central Italy sequence. The Seismic Record 1 (1), 11–19. https://doi.org/10.1785/0320210001.

Taner, M.T., Wagner, D.E., Baysal, E., Lu, L., 1998. A unified method for 2-D and 3-D refraction statics. Geophysics 63 (1), 260–274. https://doi.org/10.1190/1.1444320.

Unsworth, M.J., Malin, P.E., Egbert, G.D., Booker, J.R., 1997. Internal structure of the San Andreas fault zone at Parkfield. California, Geology 25, 359–362.

Valoroso, L., Chiaraluce, L., Piccinini, D., Di Stefano, R., Schaff, D., Waldhauser, F., 2013. Radiography of a normal fault system by 64,000 high-precision earthquake locations: the 2009 L'Aquila (Central Italy) case study. J. Geophys. Res. Solid Earth 118, 1156–1176. https://doi.org/10.1002/jgrb.50130.

Veeken, P.C.H., 2007. Seismic stratigraphy, basin analysis and reservoir characterization. In: Handbook of Geophysical Exploration. Elsevier, p. 509 (ISBN 9780080453118.).

Villani, F., Tulliani, V., Sapia, V., Fierro, E., Civico, R., Pantosti, D., 2015. Shallow subsurface imaging of the Piano di Pezza active normal fault (Central Italy) by high-resolution refraction and electrical resistivity tomography coupled with time-domain electromagnetic data. Geophys. J. Int. 203 (3), 1482–1494. https://doi.org/10.1093/gji/ggv399.

Villani, F., Improta, L., Pucci, S., Civico, R., Bruno, P.P., Pantosti, D., 2017. Investigating the architecture of the Paganica Fault (2009 M_w 6.1 earthquake, Central Italy) by integrating high-resolution multiscale refraction tomography and detailed geological mapping. Geophys. J. Int. 208 (1), 403–423. https://doi.org/10.1093/gji/ggw407.

Villani, F., Sapia, V., Baccheschi, P., Civico, R., Di Giulio, G., Vassallo, M., Marchetti, M., Pantosti, D., 2019. Geometry and structure of a fault-bounded extensional basin by integrating geophysical surveys and seismic anisotropy across the 30 October 2016 M_w 6.5 earthquake fault (Central Italy): the Pian Grande di Castelluccio basin. Tectonics 38, 26–48. https://doi.org/10.1029/2018TC005205.

Villani, F., Maraio, S., Bruno, P.P., Improta, L., Wood, K., Pucci, S., Civico, R., Sapia, V., De Martini, P.M., Brunori, C.A., Doglioni, C., Pantosti, D., 2021. High-resolution seismic profiling in the hanging wall of the southern fault section ruptured during the 2016 Mw 6.5 Central Italy earthquake. Tectonics 40 (9). https://doi.org/10.1029/2021TC006786 e2021TC006786.

Faure Walker, J., Boncio, P., Pace, B. et al. Fault2SHA Central Apennines database and structuring active fault data for seismic hazard assessment. *Sci Data* **8**, 87 (2021). https://doi.org/10.1038/s41597-021-00868-0.

Everett, M.E., 2013. Near-Surface Applied Geophysics, Cambridge University Press, Online ISBN:9781139088435, https://doi.org/10.1017/CBO9781139088435.

Wathelet, M., Chatelain, J.L., Cornou, C., Di Giulio, G., Guillier, B., Ohrnberger, M., Savvaidis, A., 2020. Geopsy: a user-friendly open-source tool set for ambient vibration processing. Seismol. Res. Lett. 91 (3), 1878–1889. https://doi.org/10.1785/0220190360.

Whittaker, A.C., M. Attal, P.A. Cowie, G.E. Tucker, and G. Roberts (2008), Decoding temporal and spatial patterns of fault uplift using transient river long profiles, *Geomorphology*, 100, 506–526, doi:10.1016/j.geomorph.2008.01.018.

Manighetti, I., G.C.P. King, Y. Gaudemer, C.H. Scholz, and C. Doubre (2001), Slip accumulation and lateral propagation of active normal faults in Afar, *J. Geophys. Res.*, 106(B7), 13667–13696, doi:10.1029/2000JB900471.

Wilkinson, M., Roberts, G.P., McCaffrey, K., Cowie, P.A., Walker, J.P.F., Papanikolaou, I., et al., 2015. Slip distributions on active normal faults measured from LiDAR and field mapping of geomorphic offsets: an example from L'Aquila, Italy, and implications for modelling seismic moment release. Geomorphology 237, 130–141. https://doi.org/10.1016/j.geomorph.2014.04.026.